

1 **The Effect Of An Equatorial Continent On The Tropical Rain Belt. Part 2:**

2 **Summer Monsoons**

3 Michela Biasutti*, Spencer Hill,

4 *Lamont-Doherty Earth Observatory of Columbia University, 61 Route 9W, Palisades, NY 10964.*

5 Aiko Voigt

6 *Department of Meteorology and Geophysics, University of Vienna, Austria.*

7 **Corresponding author address: Lamont-Doherty Earth Observatory of Columbia University, 61*

8 *Route 9W, Palisades, NY 10964.*

9 *E-mail: biasutti@ldeo.columbia.edu*

ABSTRACT

10 The TRACMIP ensemble includes slab-ocean aquaplanet control simula-
11 tions and experiments with a highly idealized narrow tropical continent (0-
12 45°W; 30°S - 30°N). We compare the two setups to contrast the characteristics
13 of oceanic and continental rain bands and investigate monsoon development
14 in GCMs with CMIP5-class dynamics and physics. Over land, the rainy sea-
15 son occurs close to the time of maximum insolation. Other than in its timing,
16 the continental rain band remains in an ITCZ-like regime akin deep-tropical
17 monsoons, with a smooth latitudinal transition, a poleward reach only slightly
18 farther than the oceanic ITCZ's (about 10°), and a constant width throughout
19 the year. This confinement of the monsoon to the deep tropics is the result of
20 a tight coupling between regional rainfall and circulation anomalies: ventila-
21 tion of the lower troposphere by the anomalous meridional circulation is the
22 main limiting mechanism, while ventilation by the mean westerly jet aloft is
23 secondary. Comparison of two sub-sets of TRACMIP simulations indicates
24 that a low heat capacity determines, to a first degree, both the timing and the
25 strength of the regional solstitial circulation; this lends support to the choice
26 of idealizing land as a thin slab ocean in much theoretical literature on mon-
27 soon dynamics. Yet, the timing and strength of the monsoon are modulated
28 by the treatment of evaporation over land, especially when moisture and ra-
29 diation can interact. This points to the need for a fuller exploration of land
30 characteristics in the hierarchical modeling of the tropical rain bands.

31 **1. Introduction**

32 The last twenty years have seen much progress towards a theory of monsoon circulations (Geen
33 et al. 2020). It has become apparent that individual regional monsoons should not be regarded
34 as the product of local land-sea contrast (Gadgil 2003), but rather elements of a coherent global
35 monsoon (Wang and Ding 2008), integral parts of the planetary Hadley circulation and of the
36 intertropical convergence zone (ITCZ). This recognition has lead to theories of monsoons that rely
37 only on zonal mean dynamics (Bordoni and Schneider 2008; Schneider et al. 2014). Nevertheless,
38 for the zonal circulation to achieve its solstitial, approximately angular-momentum-conserving
39 regime the surface boundary must have low heat capacity (Geen et al. 2019). On Earth, this
40 means: that continents are necessary; that the oceanic ITCZ would not behave as the observed
41 zonal mean rain band behaves; and that, instead, the regional monsoons shape the seasonality
42 of the zonal mean circulation. These considerations imply that Earth's zonal asymmetries and
43 localized monsoons are essential to the zonal mean circulation (Dima et al. 2005; Shaw et al. 2015).
44 Recently, Geen et al. (2019) have argued that there exist two classes of monsoon circulations, one
45 that behaves more like a canonical ITCZ, with smooth seasonal transitions and weaker overturning
46 circulation, and one that is characterized by abrupt onset and an angular-momentum conserving
47 cross-equatorial cell. In the first class are those monsoons that are confined to about 10 degrees of
48 the equator (such as the West African and the Australian monsoon), in the second class are those
49 monsoons that are centered at more subtropical locations (e.g., the Indian monsoon). But what
50 determines the location of monsoon rainfall? We still lack a theory of the tropical rain bands that
51 is complete enough to predict this from first principles (Biasutti et al. 2018; Hill 2019).

52 The Tropical Rain belts with an Annual cycle and Continent Model Inter-comparison Project
53 (TRACMIP, Voigt et al. 2016) was implemented to addresses the relationship between monsoons

54 and the ITCZ in a set of climate models with CMIP5-class dynamics and physical parameteri-
55 zations. The experimental design *assumes* that the presence of a tropical continent will generate
56 a monsoon: the control set up is a slab-ocean aquaplanet while the monsoon set up includes an
57 idealized rectangular continent straddling the equator. In a companion paper (Biasutti et al. 2021)
58 we focused on how the regional monsoon circulation affected the annual mean state of the ITCZ.
59 In this paper, we focus on the monsoon circulation itself.

60 The first task of this study is to compare the simulated continental and oceanic rain bands to
61 each other and to measures of the monsoon and ITCZ “regimes”. Does the continental rain band
62 in TRACMIP show an enhanced poleward movement (Geen et al. 2019) or extent (Gadgil 2003)?
63 Does it transition between the dry and rainy seasons with the rapidity of a monsoon (Bordoni and
64 Schneider 2008) or the smoothness of an ITCZ (Geen et al. 2019)? How sensitive is the spatial
65 extent of the monsoon to commonly used definitions based on wind (Ramage 1971), or rainfall
66 (Webster et al. 1998; Wang and Ding 2008)?

67 As we will show (for example in Figure 1a,b), the continental rain band remains confined to
68 the deep tropics (even though the continent itself extends into subtropical latitudes) and evolves in
69 an “ITCZ-like” regime reminiscent of the West African monsoon. In today’s Africa, the limited
70 reach of the monsoon is ascribed primarily to the presence of the desert to the north, which both
71 reduces the energy input absorbed by the atmospheric column (Charney 1975; Chou and Neelin
72 2003) and is the source of low moist static energy (MSE) advected by the regional circulation (Hill
73 et al. 2017). The TRACMIP set up, though, does not include deserts, and thus the confinement of
74 the monsoon has a different origin. The second task of this study is to determine what that is.

75 It has been argued that the poleward reach of the tropical rainfall is limited by influxes of low
76 MSE (the literature refers to this process as “ventilation”, expanding on the original meaning of
77 the term in Chou et al. 2001). In Earth-like planets, the connection between rainfall and MSE

78 is qualitatively understood in terms of two processes fundamental to tropical dynamics: the verti-
79 cal mixing due to moist convection and the horizontal temperature homogenization due to gravity
80 waves. Convective Quasi Equilibrium theory (CQE, Emanuel et al. 1994) postulates, in its sim-
81 plest form, that convection relaxes the full tropospheric column to a neutrally stable profile. The
82 strongest convection warms the column the most and, as the warming is homogenized in the free
83 troposphere, increases the stability of the entire tropics (Sobel and Bretherton 2000; Chou and
84 Neelin 2004; Zhang and Fueglistaler 2020). Thermodynamics would therefore predict that max-
85 imum rainfall in the tropics coincide with maximum sub-cloud MSE (Chou and Neelin 2004)
86 and, moreover, a proportionality between the two quantities (Hurley and Boos 2013; Smyth and
87 Ming 2021). Complications arise because of entrainment, downdrafts, and differences in relax-
88 ation times between the lower (and moister) and upper (and dryer) troposphere (e.g., Arakawa
89 and Schubert 1974; Raymond 1995; Kuang 2010; Tulich and Mapes 2010). This leads to the need
90 to consider MSE above the boundary layer and the column integrated MSE, therefore, becomes a
91 useful bulk diagnostic for rainfall (e.g., Chou et al. 2001; Chou and Neelin 2003; Hill et al. 2017).

92 For both oceanic and continental tropical rain, an influx of low MSE (what we have termed
93 ventilation) can come from the colder midlatitudes (e.g., Chiang and Bitz 2005; Kang et al. 2008;
94 Peterson and Boos 2020)—unless the airflow is blocked by mountains, as is the case for the Indian
95 monsoon (e.g., Boos and Kuang 2010). For the regional monsoons, low MSE can additionally
96 come from dry deserts (Hill et al. 2017) or cool oceans (Chou et al. 2001). Land borders are there-
97 fore a key control of ventilation. TRACMIP’s design does not include different land geometries:
98 our investigation is limited to a continent 45° wide in longitude and confined to latitudes between
99 30° N and S. We should not expect, a priori, that our results will apply to different continental
100 configurations, such as subtropical continents. On the other hand, the idealized studies that have
101 linked the spatial distribution of monsoon rainfall to land geometry (Chou et al. 2001; Maroon

102 and Frierson 2016; Zhou and Xie 2018; Hui and Bordoni 2021) are limited to one or two models
103 and typically idealize the atmosphere severely, either by including only deep vertical modes in
104 the circulation, or by using simplified convection, clouds, and radiation schemes. TRACMIP's
105 full-dynamics, full-physics, multi-model framework thus provides an important complementary
106 assessment of the mechanism of ventilation and its effect on monsoon extent.

107 Chou et al. (2001), using a continental geometry similar to TRACMIP's, ascribed the limited
108 monsoon extent to the transport into the eastern domain of cool, marine air by a combination
109 of the mean westerlies and an interactive "Rodwell-Hoskins" Rossby wave emanating from the
110 monsoon rainfall itself. Their atmospheric model (QTCM, Neelin and Zeng 2000) only allowed
111 for the barotropic and the first baroclinic mode of circulation, so both the mean westerlies and
112 the anomalous circulation were features of the free troposphere. Zhou and Xie (2018), using a
113 model with simplified physics but fully resolved vertical structure, also explained the ventilation
114 of a simplified zonally confined continent in terms of the free tropospheric westerlies. Specifically,
115 they claimed that westerlies bring colder temperature from the ocean over the continent and, as
116 convection homogenizes the cooling down to the surface, they end up stabilizing the atmosphere
117 and reducing rainfall. But conclusions from these earlier studies might depend on their severe
118 idealizations of the atmosphere and, indeed, they seem at odds with our previous results in Biasutti
119 et al. (2021): in TRACMIP, land influences the ocean downstream via boundary-layer winds, the
120 anomalous circulation is important, and so are moist radiative feedbacks. Therefore, we examine
121 in detail the mechanisms of monsoon ventilation.

122 While the atmosphere in the TRACMIP models is simulated with full physics and full dynamics,
123 the land surface is extremely idealized: the "continent" consists of modified slab-ocean aquaplanet
124 grid cells with increased evaporative resistance, increased albedo, reduced heat capacity, and no
125 ocean heat transport (as specified by q -fluxes). TRACMIP was not purposefully designed to ex-

126 plore the role of different idealizations, but fortuitous errors of implementation allow us to gain
127 insight on the effects of each land characteristics. We have shown in Biasutti et al. (2021) that
128 changes in heat capacity play a predominant role in the creation of solstitial anomalies over land
129 and even of the annual mean anomalies over the ocean. Here, we again compare simulations
130 where the continent has either reduced or unchanged heat capacity to show how the latter affects
131 the continental rain band, in comparison to other land characteristics.

132 This paper is organized as follows. In Section 2 we describe in more details the model simu-
133 lations and our analysis procedures. The following three sections contain the bulk of our results.
134 First (Section 3), we provide an overview of the seasonal changes in the LandControl simulations
135 and characterize the behavior of the oceanic and continental rain bands in terms of a set of descrip-
136 tive measures of the monsoon and ITCZ “regimes”. Second (Section 4), we provide more detail
137 on the spatial pattern and poleward reach of the precipitation anomalies over the summer continent
138 and we investigate whether ventilation is achieved by free-tropospheric or boundary-layer winds
139 and by the mean or the anomalous circulation. And third (Section 5), we clarify the importance
140 of a reduced heat capacity in driving the continental anomalies. Section 6 summarizes our results,
141 discusses them in connection to previous idealized modeling of the monsoon, and provides our
142 outlook for future research.

143 **2. Data and methods**

144 *a. The TRACMIP protocol*

145 Table 1 provides a list of TRACMIP models (Voigt et al. 2016) included in this study. All of
146 the models include clouds and water vapor-radiation interactions, except the CaltechGray model,
147 which assumes a fixed emissivity in the atmosphere and contains no clouds (Bordoni and Schnei-

148 der 2008). We compare AquaControl and LandControl simulations. AquaControl is an aquaplanet
149 configuration with a slab ocean of 30m depth, zero eccentricity, atmospheric CO₂ concentrations
150 of 348 ppmv, and a prescribed ocean heat transport convergence that is an idealized version of
151 the observed zonal mean and that is the only source of asymmetry in the simulations under con-
152 sideration. Because of this ocean heat flux, the NH is warmer than the SH in the annual mean.
153 LandControl includes an idealized continent 45 degrees wide in longitude and extending in lati-
154 tude from 30°N to 30°S. The idealization of land properties is accomplished by modifying ocean
155 grid cells in the following ways: (1) the q -fluxes representing ocean heat transport convergence are
156 zeroed out in the continent region (note that a uniform compensation over the ocean ensures zero
157 net energy flux anomaly in the global mean); (2) the surface albedo over the continent is increased
158 by 0.07, corresponding to vegetated land; (3) the evaporation rate coefficient in the bulk moisture
159 flux equation is halved, representing enhanced evaporative resistance by vegetation; and (4) the
160 heat capacity is reduced by changing the mixed layer depth from 30 m (similar to the tropical
161 mean mixed layer depth and appropriate to achieve an Earth-like annual cycle in the aquaplanet
162 configuration) to 0.1 m (representative of a shallow layer of moist soil).

163 We focus on the models that followed protocol exactly (hereafter, the protocol models; see the
164 correction to Voigt et al. (2016) and discussion in Biasutti et al. (2021)), but we also briefly present
165 results from models that incorporated the first three properties of land, but did not reduce the heat
166 capacity of the continental region (hereafter, the MetUM models). We compare the MetUM to
167 the protocol models in order to isolate the anomalies due to the choice of mixed layer depth from
168 those due to other land characteristics. To ensure that our interpretation is correct, and that model
169 choice is not an issue, we ensure that the inter-model scatter across the protocol models is much
170 smaller than the difference between the protocol models and the MetUM models.

171 *b. Rain Bands Diagnostics*

172 We refer to zonal-mean quantities as “rain bands”, with the understanding that the zonal average
173 is calculated from global data in the AquaControl simulations and over just the continent (0-45W)
174 in the LandControl simulations. Land and ocean climatologies differ substantially in how fast
175 either one responds to the external forcing coming from seasonally varying insolation. Therefore,
176 LandControl–AquaControl differences emphasize the changes in the timing of the rainy season at
177 any given latitude. If, instead, we compare the rain bands in their respective rainy seasons, we
178 emphasize differences in structure and behavior, independent of timing.

179 We characterize the seasonal monsoon by either rainfall or wind and the year-round rain bands in
180 terms of their spatial extent, position, rapidity of their meridional displacement and characteristics
181 of their ascent (vertical profiles, frequency, and intensity). Specifically, we define the monsoon
182 regions and describe the rain bands according to the metrics summarized below:

183 **Monsoon Rainfall** Following Wang and Ding (2008), we define monsoon regimes where (a) the
184 local summer-minus-winter precipitation rate exceeds 2 mm day^{-1} and (b) the local summer
185 precipitation exceeds 55% of the annual total. The first criterion distinguishes the monsoon
186 climate from more arid climate regimes. The second ensures that precipitation is concentrated
187 during local summer, thereby distinguishing the monsoon climate from equatorial perennial
188 rainfall regimes. We define summer differently in the case of LandControl and AquaControl.
189 For LandControl we take local summer to denote May through September for the NH and
190 November through March for the SH. AquaControl seasons are shifted by three months (NH
191 summer goes from August to December and SH summer from February through June).

192 **Wind Reversal** We identify regions of wind reversal as those regions where the maximum dif-
193 ference in wind direction for any pair of months is larger than 90 degrees, for non-negligible
194 wind speed (the exact value of the threshold is unimportant) .

195 **Rainband Position** We calculate the position of the rain band as the centroid of precipitation
196 following the definitions of Adam et al. (2016) and Voigt et al. (2014)¹, or as the latitude of
197 maximum rainfall.

198 **Rainband Migration Speed** We take the time derivative of the 5-day running-mean smoothed
199 daily values of the rain band position to calculate the meridional translation speed of the rain
200 bands (Geen et al. 2019)

201 **Rain Band Width** Following Byrne and Schneider (2016), we define the width of the rain bands
202 as the meridional distance where net precipitation (precipitation - evaporation, P-E) is posi-
203 tive.

204 **Rain Characteristics** We diagnose changes in rainfall characteristics in terms of frequency of
205 rainy days (rain accumulation larger than 1mm day^{-1}) and simple daily rain intensity (rain
206 intensity on rainy days in mm day^{-1}).

207 We use climatologies based on the last 20 years of monthly data or, when daily data are necessary,
208 on 10 years of simulations.

¹The Adam et al. (2016) definition calculates the precipitation- and area-weighted mean of latitude between 30°N and S; the Voigt et al. (2014) definition calculates the latitude at which the area-integrated precipitation (within the same tropical band) that falls to its north equals the area-integrated precipitation that falls to its south. The former definition is more weighted toward rainfall away from the equator and indicates a smaller seasonal excursion than the latter definition.

209 *c. Other Diagnostics*

210 We link the position of the rain bands to simple diagnostics of the horizontal gradients in the
211 low-level atmosphere. Specifically, we calculate the latitude of the zonal or sector mean of:

212 **Inter-Tropical Front** : the minimum in sea level pressure. This is equivalent to the locus of
213 surface mass convergence and it is expected to be tightly related to boundary layer moisture
214 convergence in the absence of strong moisture gradients.

215 **925hPa MSE maximum** : a measure of the sub-cloud layer MSE maximum. From a purely
216 thermodynamic perspective, this quantity should coincide with maximum rainfall (see In-
217 troduction). Dynamic considerations, instead, require that maximum surface MSE limit the
218 poleward extent of the overturning cell, so that maximum vertical motion and, thus, rain-
219 fall remain on the equatorward flank (see Privé and Plumb (2007) for a derivation based on
220 axisymmetric theory and Singh (2019) for an extension).

221 **Surface Temperature maximum** : the connection between SST and rainfall is not direct, but
222 instead it is mediated by sea level pressure (Lindzen and Nigam 1987; Back and Bretherton
223 2009) and MSE (Emanuel et al. 1994; Hurley and Boos 2013). Yet it remains a commonly
224 used and useful diagnostic (Biasutti et al. 2021; Wei and Bordoni 2018) and we report it here.

225 We use climatologies based on the last 20 years of monthly data.

226 **3. Monsoon and ITCZ regimes: Diagnostics of Oceanic and Continental Rain Bands**

227 Figure 1 shows the month-latitude Hovmöller diagrams of climatological fields that have been
228 zonally averaged over the oceanic and continental sectors in the LandControl simulations; con-
229 tours of the AquaControl climatology (zonally averaged) are superimposed on the LandControl
230 sector averages in order to help the comparison. Besides the rain bands (Figure 1a,b), we show the

231 seasonal evolution of surface temperature (Figure 1c,d), and low-level MSE (Figure 1e,f). The cli-
232 matology of the LandControl simulation averaged over the ocean sector (left panels, Figure 1a,c,e)
233 is similar to the zonal mean of AquaControl, with only small differences in the timing and inten-
234 sity of peak anomalies in all fields. This similarity is consistent with our findings in Biasutti et al.
235 (2021), in which we show that the influence of land extends only about 120° to the west of the
236 continent, leaving most of the ocean unaffected. In what follows, we select to contrast directly the
237 oceanic rain band in the AquaControl and the continental rain band in the LandControl.

238 The most obvious difference between LandControl and AquaControl, and the expected result of
239 a reduced surface heat capacity, is that the annual cycle is phase-shifted early over land, compared
240 to the ocean, by between 1 and 2 months in all variables (right panels, Figure 1b,d,f). Peak
241 values are also affected by land characteristics, but differently for different fields. Precipitation
242 shows a small reduction in peak values, especially in the Northern Hemisphere. The surface
243 temperature summer-to-winter seasonal excursions are of larger magnitude in LandControl than
244 in AquaControl (as is also expected for a lower heat capacity system forced by oscillating heat
245 fluxes). In contrast, seasonal MSE excursions remain similar across ocean and land, but MSE is
246 overall reduced in LandControl. A lesser MSE maximum derives from the imposed reduction in
247 local evaporation and also from transport of low MSE into the continent (see also Sec. 4).

248 The impression one derives from Figure 1 is that the oceanic and continental rain bands are over-
249 all very similar – aside from their phasing within the calendar year. Following Geen et al. (2019),
250 we suggest that the TRACMIP monsoon is in a deep-tropical, ITCZ-like regime, namely a regime
251 in which the monsoon never jumps to subtropical latitudes and never develops an approximately
252 angular momentum conserving circulation. Yet, the behavior of the land-based rain band remains
253 distinct from that of the oceanic ITCZ.

254 More detailed analysis supports this suggestion. Figure 2 shows the seasonal migration of the
255 rain band (indicated by three definitions in different shades of blue), alongside the location of
256 maximum surface temperature (red), maximum boundary layer MSE (magenta), and minimum
257 sea level pressure (black). In AquaControl, the maxima of surface temperature and MSE linger
258 at their northernmost and southernmost positions and transition between the two rather quickly,
259 more like square waves than sinusoids. The rain band moves between latitudes in a manner that is
260 more gradual, but also more asymmetric: the shift from South to North is quicker than the reverse.
261 Thus, over ocean, the relationship between the rain band and the position of the maximum MSE
262 varies over the course of the seasonal march.

263 We have already noted that the evolution of the continental climate is shifted early. We now see
264 that, in the NH, the timing of extrema in surface temperature, MSE, and SLP shifts more (from
265 October to August) than that of the rain band (from October to September). In the SH, both the
266 rain band and the surface extrema shift by the same amount, two months. Thus, the northward
267 migration and the southward migration are now of the same duration. Moreover, while the loci of
268 extreme temperature, MSE, and SLP are experiencing larger meridional excursion over land than
269 over ocean, the rain band is not: it oscillates between 5°S and 10°N over both land and ocean.
270 This causes a larger separation between the rain band and surface extrema (temperature, MSE,
271 SLP) over land, compared to the ocean. A separation of the rain band from the maximum in MSE
272 is expected from theories of the zonally symmetric moist circulation, especially for ITCZs located
273 off the equator (Priv and Plumb 2007) but within the tropics (Singh 2019). Nevertheless, it is
274 unclear why the magnitude of this displacement would be larger over land, given that the location
275 of the rain band is similar in the two domains. A larger separation between the rain band and the
276 ITF, compared to that seen over ocean, is a feature of real world monsoons, most famously in West
277 Africa and Australia (Nicholson 2018; Nie et al. 2010). But the correspondence with TRACMIP is

278 only partial: in observations the ITF pushes into dry deserts and produces dry ascent and a shallow
279 circulation, while in the simulations ascent remains deep between the rain centroid and the ITF,
280 leading to rainfall. As we shall see in the next section, a zonal-mean view might be insufficient to
281 explain the meridional extent of the TRACMIP monsoon.

282 The degree of similarity in the progressions of the oceanic and continental rain bands is detailed
283 in Figure 3. The top panels reveal that both rain bands reach similar northernmost and south-
284 ernmost positions: there is less difference between the LandControl and AquaControl cases than
285 across models of the ensemble or across two commonly used centroid definitions. The transla-
286 tion speeds (shown in Figure 3c,d for one centroid definition, but robust to the choice) are also
287 somewhat similar between ocean and land, but with some noteworthy differences. Compared to
288 the aquaplanet, migration speeds over the continent are generally faster and less consistent with
289 a perfect sinusoidal progression (shown as an ellipse calculated from the annual harmonic). The
290 onset of the land monsoon (first and third quadrants) is somewhat slower than its demise (second
291 and fourth quadrants) in opposition to the behavior of the AquaControl ITCZ and to that reported
292 for aquaplanet monsoons in Geen et al. (2019).

293 Figure 4 shows the evolution of the rain band width, as defined in Section 2. The two leftmost
294 panels show latitude-month diagrams, while the right panel shows both the summer reach of the
295 rain band in each hemisphere (vertical bars, left axis) and the maximum width of the rain band
296 over the course of the year (markers, right axis). By either of these measures, the land-based rain
297 band behaves in ways qualitatively similar to the ocean-based ITCZ, with the only difference that
298 it reaches slightly further poleward (especially in the SH) and is slightly wider throughout the year
299 (but not in all models).

300 Finally, we move past the two-dimensional view of the monsoon in Figure 5, which shows the
301 extent of the “global monsoon” as defined by the seasonality of rainfall and wind. The two defi-

302 nitions select for different regions: The rain-based monsoon region is nearly completely confined
303 to the continent, extends to the subtropics, and is more extensive in the SH (where rainfall is
304 concentrated in a shorter rainy season). The wind-based monsoon is elongated over the ocean,
305 meridionally confined to the deep tropics, and is more extensive in the NH (where the circulation
306 is stronger). The narrow extent of the wind-based definition is reminiscent of the African case. Not
307 so the rain-based definition, which selects for subtropical areas that, in observations, are deserts
308 (evaporation from a permanently moist surface in TRACMIP causes the discrepancy, as can be
309 surmised from the P-E pattern). Nevertheless, when we take the sector or zonal averages (right
310 panels), both definitions are consistent with each other and with the P-E metric in selecting for a
311 slightly broader meridional span of the LandControl rain band, compared to the AquaControl.

312 In summary, the above analysis shows that the TRACMIP monsoons is a deep-tropical monsoon
313 in an ITCZ-like regime, with some similarity to the West African monsoon. First, the width of
314 the TRACMIP rain band is similar over land and ocean and close to constant throughout the year.
315 Second, the rain's northernmost reach is similar in the two domains. Third, areas of positive P-E
316 progress smoothly from one hemisphere to the other. Again, this behavior agrees with observations
317 in the African sector: the maximum in rainfall jumps from the coastal ocean to the interior at the
318 beginning of summer (Sultan and Janicot 2003), but the zonally averaged rainfall band progresses
319 quite smoothly. Moreover, the transition over Africa is faster in its retreat than in its advance
320 (Biasutti 2019), consistent with the behavior seen in the TRACMIP LandControl.

321 **4. The poleward extent of the summer monsoon: Mechanisms of ventilation.**

322 A map view of the LandControl-AquaControl seasonal anomalies provides clues to the pro-
323 cesses that determine the extent of the TRACMIP monsoon and indicates that zonal asymmetries
324 are important. (The extent to which this conclusion depends on the narrow longitudinal extent of

325 the continent is discussed later.) Figure 6 shows the surface temperature (shaded) and precipitation
326 (contour) anomalies for the four standard seasons; the AquaControl rain band is also shown for
327 reference. Throughout the year, temperature and rainfall anomalies over land are consistent—in
328 sign and strength—with the accelerated response of the continent to insolation (compared to the
329 ocean) and with the tendency for rainfall to follow the net energy input into the atmosphere. This
330 translates to small anomalies during equinox seasons (comparable to the annual mean anoma-
331 lies, Biasutti et al. 2021) and much larger anomalies during the solstice seasons. Anomalies in
332 both temperature and rainfall are positive in the summer hemisphere and negative in the winter
333 hemisphere.

334 The wintertime cold anomalies are the largest, due to the reinforcing effects of enhanced resis-
335 tance to evaporation and reduced energy input, further amplified by moist-radiative feedbacks and
336 by the divergent surface circulation (Biasutti et al. 2021). Summertime and wintertime anomalies
337 in rainfall are more comparable in their peak positive and negative values, but they differ greatly in
338 shape. The wintertime dry anomalies are centered at the latitude of the AquaControl ITCZ and are
339 roughly zonally oriented (both foregone consequences, to some degree, of no negative rainfall).
340 The summertime wet anomalies extend poleward from the latitude of the AquaControl ITCZ and
341 are characterized by a triangular pattern: they are narrow in the western part of the continent and
342 broad in the eastern part, where they reach the coastlines at 30° N and S. A similar pattern of
343 summertime rainfall anomalies has been interpreted (Chou et al. 2001; Zhou and Xie 2018) as the
344 effect of ventilation, primarily by the mean free tropospheric westerlies. We find that ventilation
345 happens by different mechanisms in TRACMIP.

346 Figure 7 shows fields relevant to ventilation in the two summer hemispheres: JJA above the
347 equator and DJF below the equator. The top and bottom panels describe processes in the free
348 troposphere and in the boundary layer, respectively. Figure 7a shows temperature anomalies at

349 300hPa (shaded), geopotential anomalies at 700hPa (contours) and the full LandControl wind at
350 700hPa (vectors). The mean westerlies are weak over the subtropical portion of the continent
351 and the temperature anomalies do not resemble what we would expect from westerly advection:
352 instead of decaying inland, they are strongest in the western part of the continent and they are
353 warm in the summer hemisphere subtropics, opposite what is necessary for ventilation (Zhou and
354 Xie 2018). Upper level temperatures are cold everywhere else and show the Gill-like signature
355 (Gill 1980) of the negative rainfall anomalies in the oceanic cold tongue. It is possible that these
356 cold temperatures are homogenized downward by convection and modulate rainfall and surface
357 temperature in the core monsoon region. Nevertheless, they do not appear to be preventing rainfall
358 in the western portion of the subtropical continent.

359 Figure 7b shows fields relevant to low-level processes (anomalies in precipitable water, bound-
360 ary layer geopotential and wind) and suggests a predominant role for such processes in limiting
361 the monsoon in the western portion of the continent and enhancing it in the East. Note, for ex-
362 ample, the correspondence between the slanted positive anomalies in precipitable water over the
363 summer continent and the low-level cyclonic circulation that brings tropical moist air to the eastern
364 continent and subtropical dry air to the western continent.

365 The above suggestions are confirmed by a quantitative analysis of MSE advection. Figure 8a,b
366 show the total MSE advection in the boundary layer and the free troposphere (925hPa and 300hPa,
367 respectively; these levels were chosen as the most clearly representative, but results are robust to
368 the choice) in the the NH hemisphere during JJA (DJF anomalies in the SH are a nearly perfect
369 mirror image of JJA in the NH and we omit them for clarity). The pattern of anomalies is sim-
370 ilar at both levels, but the magnitude of the anomalies is much larger in the boundary layer. We
371 decompose the advection in its zonal and meridional terms and further decompose those as the
372 linear combination of the advection of anomalous MSE by the mean wind and advection of mean

373 MSE by the anomalous wind. We obtain 4 terms that are plotted in Figure 8c through j. This de-
374 composition highlights how MSE advection is achieved differently at different levels. In the free
375 troposphere, the mean westerlies acting on the anomalous gradient of MSE do indeed ventilate
376 the western part of the continent, as suggested in the literature. But this effect is counteracted by
377 the other terms, especially by the advection of the climatological MSE gradient by the anomalous
378 meridional wind. Within the boundary layer, the dominant mechanism of ventilation is the advec-
379 tion of the background MSE gradient by the meridional component of the anomalous circulation.
380 The background zonal wind is most relevant at the coastlines, where it acts to counteract the main
381 advection pattern. The other terms are small over the subtropical continent. (We note as an aside
382 that the anomalous negative MSE advection that extends past the continent at about 10° N is the
383 result of the covariant term.)

384 The vertical profiles of the MSE transport terms (Figure 9) confirm the description above and
385 add some insight on the scatter across models. Higher in the troposphere, the advection into the
386 western subtropical continent of low oceanic MSE by the mean zonal wind is compensated by the
387 advection of the mean MSE by the anomalous meridional wind. Each term is uncertain across the
388 ensemble, but the cancellation is not, so that the total uncertainty in the free-troposphere ventilation
389 is low. Lower in the boundary layer, the continent is ventilated by the anomalous meridional wind
390 acting on the background gradient in MSE between the tropics and the midlatitudes. This is the
391 dominant term in the column MSE budget and imparts its uncertainty to the total advection term.

392 We conclude that, in TRACMIP, the diffusion of MSE anomalies by the free-troposphere west-
393 erlies is an active mechanism, but not the one primarily responsible for the ventilation of the
394 subtropics. The poleward extent of the monsoon rains, in its mean and its uncertainty, is predom-
395 inantly a consequence of anomalous poleward flow in the boundary layer acting on the prevailing
396 MSE field that decreases toward the pole.

397 **5. Land idealizations: The effect of a reduced heat capacity**

398 From the simplest model of a uniform surface layer forced by a sinusoidal heat source, we expect
399 that the small phase shift between insolation and surface temperature over land derives from the
400 reduced heat capacity of continental grid points. Yet, we have seen in Figures 1 and 3 that neither
401 MSE nor, especially, rainfall, covary perfectly with temperature, so that the question of the role of
402 different land characteristics on rainfall remains somewhat open.

403 To identify whether land characteristics other than heat capacity contribute to the simulated
404 LandControl-AquaControl seasonal changes, we contrast the mean anomalies across models that
405 exactly followed the TRACMIP protocol to those across the two MetUM models, in which a re-
406 duced heat capacity for land grid points was not imposed. Figure 10a,b show the latitude-month
407 Hovmöller diagrams of LandControl-AquaControl rainfall anomalies (alongside the AquaCon-
408 trol rain band, for reference). The top panel shows alternating dipoles in rainfall anomalies in
409 the protocol models, with wet anomalies preceding, and dry anomalies trailing, the AquaControl
410 rain band. The mean state and the anomalies are close to being in quadrature, suggesting a shift
411 in the seasonality and consistent with a much smaller annual-mean signal (Biasutti et al. 2021).
412 The bottom panel (in which land does not have a reduced heat capacity) shows peak anomalies
413 of similar magnitude, although the pattern is different. When idealized land retains a high heat
414 capacity, positive equatorial anomalies persist through the year and the subtropical dry anomalies
415 are limited to local summer, when they act to reduce the local maximum. Thus, the timing of the
416 rainy season remains unaffected.

417 We check the robustness of these results by examining the rainfall anomalies in the individual
418 protocol models and MetUM models averaged within the northern (Figure 11a) and southern Fig-
419 ure 11b) continent. Only the protocol models show the alternating positive and negative anomalies,

420 while the MetUM models show only dry anomalies, especially intense in correspondence of the
421 main rainy season. We note that the CAM5-Nor model (magenta line), is an outlier among the
422 protocol models, somewhat closer to the behavior of the MetUM models: drying associated with
423 land characteristics besides heat capacity (evaporative resistance, albedo, and lack of heat trans-
424 port convergence) has a more prominent role in this model. Nevertheless we will consider the
425 ensemble mean of all protocol models and interpret mean phase shifts as due to changes in heat
426 capacity.

427 Rainfall reduction in the continental subtropics occurs by different mechanisms when it is due
428 primarily to a smaller heat capacity or primarily to a resistance to evaporation. Figure 10b and
429 e show the LandControl-AquaControl changes in the frequency of rainy days in the two sets of
430 models (protocol and MetUM); Figure 10c and f show the changes in daily intensity. Peak changes
431 in intensity are around 8 mm day^{-1} , either in positive or in negative values and in both sets of
432 models. Peak changes in rain frequency are much larger in the case of the protocol models, and
433 much larger for negative than for positive anomalies. This asymmetry is consistent with the more
434 pronounced wintertime circulation changes driven by the heat capacity-induced land-sea contrast
435 (Figure 6, see also Biasutti et al. (2021) for a comparison with the MetUM models) and with a
436 greater role for dynamics, as opposed to thermodynamics, in affecting the occurrence of rainy days
437 rather than their intensity. In contrast, in the MetUM simulations, the imposed land characteristics
438 do not create large circulation in and out of the continent and changes in rainfall are predominantly
439 caused by thermodynamic properties and expressed as changes in intensity.

440 A reduced heat capacity also affects the profile of ascent in the rain band (Figure 12). Fig-
441 ures 12a,c show the latitude/pressure zonal and sector mean of vertical velocity for the SH summer
442 (DJF in LandControl and MAM in AquaControl in the case of the protocol models, MAM in both
443 LandControl and AquaControl in the case of the MetUM models). Figures 12b and d show each

444 model's profile in the ascent regions. For models with a reduced heat capacity over land, vertical
445 ascent is larger in magnitude and much more top heavy over land than over ocean². The omega
446 profile remains unchanged in the case when land does not have a reduced heat capacity. This
447 change in the vertical profile of ascent only depends on the different heat capacity of the lower
448 boundary, not on where the rain band is in its seasonal march. It follows that the presence of a low
449 heat capacity continent will influence the responsiveness of the rain band to MSE fluxes: deeper
450 or shallower profiles of ascent are associated with larger or smaller moist stability (Raymond et al.
451 2009), thus modulating the relationship between the position of the rain band and MSE transport
452 (see, e.g., Biasutti et al. 2018). It should be noted, though, that the difference in ascent profile
453 between the (low-heat capacity) land and the ocean is not due to the difference in the local heat
454 capacity per se, but derives from changes in the large scale circulation. This can be surmised from
455 the comparison of the profile ascent in the western third of the continent with that over the eastern
456 third of the continent, which show markedly different features (not shown). In the East, where the
457 low level flow is extending the monsoon poleward, the profile of ascent is roughly constant, with a
458 weak maximum at about 600hPa, similar to the oceanic profile in Figures 12a,b. In the West, where
459 the low level flow ventilates the continent, the profile of ascent has, in most models, two distinct
460 maxima at 850hPa and 300hPa, an accentuated version of the land profile in Figures 12a,b. This
461 structure is suggestive of a bimodal distribution of convective motions: either weak and capped
462 at low level by the dry flow or, when CAPE is finally released, deep and intense. This results
463 have a nice correspondence with those of Smyth and Ming (2021), who also find differences in the
464 vertical profile of ascent in idealized simulations of the South American monsoon, depending on
465 the characteristics of the surface. In their case, shallow ascent corresponded to a dry surface and

²The NorESM model is an exception, but we have not adjusted the averaging period to match its continental summer; when that is done, it too has deeper ascent over land

466 deep ascent to a wet surface. The more realistic land surface, with a bucket model of soil moisture,
467 presented a double maxima reminiscent of a mixture of the two soil moisture end members.

468 **6. Summary and Discussion**

469 In this paper we have examined the rain band that develops over the idealized tropical conti-
470 nent in the LandControl simulations of the TRACMIP multi-model ensemble (Voigt et al. 2016).
471 The continental rain band moves farthest poleward around summer solstice, 1-2 months preceding
472 its oceanic counterpart. Whereas the rain band width, translation speed, and maximum rain rate
473 differ modestly between land and ocean. Previous work (Geen et al. 2019) had suggested that
474 subtropical monsoons abruptly develop an approximately angular-momentum conserving circu-
475 lation, while those in which maximum rainfall remains within about 10° or 15° of the equator
476 show a weaker, smoothly changing circulation (dubbed an ITCZ-like regime). This distinction
477 motivated our investigation of the mechanisms of ventilation that set the poleward reach of the
478 TRACMIP monsoon. We find that the advection of low MSE into the subtropical land by the
479 low-level anomalous meridional wind acting on the background distribution of moist static energy
480 is the predominant mechanism, while the advection of anomalous MSE by the mean westerlies is
481 secondary. This means that what sets the anomalous circulation sets the position of the rainfall
482 maximum. The opposite is also true: the position of the rainfall maximum modifies the circulation
483 (directly, Rodwell and Hoskins (1996); Chou et al. (2001), or by bringing the circulation into an
484 approximately angular-momentum conserving regime, Geen:2019fy). Together, these conditions
485 signify a tight coupling between rainfall and circulation, more so in TRACMIP than in previous
486 studies in which the effect of the background circulation was paramount.

487 These insights are helpful to assess idealized simulations of the tropical rain bands: what is
488 retained and what is lost when a study eliminates a process or an entire component of the climate

489 system? To begin to answer this question we focus on how different idealizations play out in our
490 study and in the broader theoretical literature on the the global monsoon and ITCZ.

491 *(i) Vertical Wind Structure.* The pivotal studies of Chou et al. (2001) and Chou and Neelin (2003)
492 were carried out with QTCM-1, the first version of the Quasi-equilibrium Tropical Circulation
493 Model (Neelin and Zeng 2000; Sobel and Neelin 2006). In its original formulation, QTCM sim-
494 plified the vertical structure of the atmosphere to one with full-troposphere overturning cells and
495 no boundary layer dynamics. By design, therefore, ventilation was the effect of bulk advection of
496 mid-latitude oceanic low-MSE air by the column-integrated westerlies in both the basic state and
497 the anomalous circulation (itself a product of the monsoonal rainfall, as in the work of Rodwell
498 and Hoskins 1996). While the distribution of land rainfall in TRACMIP is not qualitatively dif-
499 ferent from that in QTCM, boundary-layer advection of low MSE by the anomalous meridional
500 circulation is the key process. The advection by the free troposphere mean westerlies is an active
501 process, but secondary, and mostly counteracted by meridional advection.

502 One caveat remains necessary: while the TRACMIP GCMs resolve the boundary layer and
503 the ventilation by the low-level flow, they do not reproduce a continent-wide shallow meridional
504 circulation similar to the ones that affect the African and Australian monsoons (e.g., Nie et al.
505 2010). These regions experience dry ascent poleward of the rainband; instead the TRACMIP
506 continent experience rainfall in all regions of surface ascent. Consistent with the literature on heat
507 lows (Rcz and Smith 1999) and monsoon extent (Chou and Neelin 2003; Smyth and Ming 2021),
508 we attribute this to the fact that the idealized continent has low albedo and only a partial moisture
509 limitation. Nevertheless, the western region of the continent provides an analog for the interaction
510 between the rain band and the shallow circulation and supports the notion that such interaction is
511 significant (Hill et al. 2017; Shekhar and Boos 2017; Zhai and Boos 2017). Besides limiting the

512 extent of the monsoon, the dry northerly flow appears to changes the profile of ascent, making it
513 less ocean-like and more consistent with the build up of CAPE and the occurrence of more intense
514 deep convection.

515 *(ii) Continental Geometry.* We have not investigated land geometry per se, but we have demon-
516 strated a primary role for the low-level circulation in ventilating the monsoon, and we can speculate
517 on how the continental geometry would matter, at least for equatorial continents. First of all, we
518 can assume that a continent that extended poleward into the region of surface westerlies would be
519 responsive to those as well (just as the TRACMIP ocean responds to the advection by the mean
520 easterlies, Biasutti et al. 2021). Second, because northerly MSE advection is key, a continent
521 that extended into colder oceans, or that included a desert to its poleward flank, would experi-
522 ence greater ventilation. We do not see a straightforward extension of our results to subtropical
523 continents, with ocean on their equatorial boundaries, and thus we can only refer to the relevant
524 literature for such case (see Maroon and Frierson 2016; Zhou and Xie 2018; Hui and Bordoni
525 2021, among others)

526 We can also speculate on the effect of the width of the continent (again, for the case of a conti-
527 nent straddling the equator). Zhou and Xie (2018) suggested that the length scale of the oceanic
528 influence over land is given by a balance between the time scales of upper-level advection and
529 convective mixing. But their view presupposes that westerly cold advection is the predominant
530 mechanism of ventilation. If boundary layer processes are instead predominant, the scale of the
531 low-level continental low becomes key. How the latter depends on local and remote rainfall and
532 cloud anomalies, as well as on the characteristics of the lower boundary, remains an open question.

533 *(iii) Surface Evaporation.* Previous literature has shown that the treatment of evaporation over
534 land modulates the extent of the monsoon in several key ways, and results from TRACMIP add

535 some detail to this view. Continental rainfall decreases with increased moisture limitation (Chou
536 et al. 2001; Smyth and Ming 2021, although the latter study finds substantial rainfall even for
537 dry land surface) as well as with decreased MSE (Hurley and Boos 2013). We interpret these
538 relationships to mean that impaired evaporation makes continental rainfall more sensitive to ven-
539 tilation. Based on the similar monsoon limitations in the Chou et al. (2001) and Smyth and Ming
540 (2021) studies (where a bucket model mimicked soil moisture processes) and TRACMIP (where
541 an evaporative resistance crudely mimicked vegetation) we speculate that, as long as evaporation
542 is reduced over land, the means of such reduction might not be a crucial choice. Second, reduced
543 evaporation contributes to the asymmetry between continental winter cooling and summer warm-
544 ing and to the drying of the equatorial ocean (Biasutti et al. 2021), modulating surface temperature
545 and pressure gradients. Therefore, we expect that the strength and the structure of the low-level
546 circulation anomalies that ventilate the monsoon would depend on the amount of evaporation at
547 the land surface. Third, the absence of a dry shallow circulation in TRACMIP supports the hy-
548 pothesis that a subtropical desert is necessary for the development of a continent-wide heat low
549 and to the longitudinal extension of the northerly ventilation across the monsoon.

550 *(iv) Moist Radiative Processes.* Influential studies of the rain bands (ITCZ and monsoons, e.g.,
551 Bordoni and Schneider 2008; Bischoff and Schneider 2014; Zhou and Xie 2018, among many)
552 have been carried out with a model (Frierson et al. 2007) that simplified atmospheric physics, and
553 in particular did not include the radiative effects of water vapor and clouds. Reassuringly, the same
554 model is shown here to behave consistently with the ensemble of protocol models. Nevertheless,
555 the CALTECH model (with no moist-radiative feedbacks; Bordoni and Schneider 2008) and the
556 NorESM model (with strong moist-radiative feedbacks; Biasutti et al. 2021) often stand out as
557 outliers. This supports the conclusion of many previous studies (for example, Kang et al. 2009,

558 Maroon and Frierson 2016, Byrne and Zanna 2020, Biasutti et al. 2021 and, for a comprehensive
559 review, Voigt et al. 2021) that moist-radiative processes affect the dynamics of the tropical rain
560 bands in important ways, albeit they might not alter their dynamics in a fundamental, qualitative,
561 way.

562 *Outlook.* The above discussion points to the need to better formalize a modeling hierarchy for
563 land. For other GCM components besides land, there is a recognized hierarchy of model complex-
564 ity from which researchers can choose the level best suited to their objectives. For example, the
565 ocean can be represented with fixed (uniform or non-uniform) surface temperatures, a slab with
566 specified q -fluxes, a column ocean, or a full dynamical ocean (Jeevanjee et al. 2017). It is not
567 obvious what the equivalent hierarchy should look like for land models since there are so many
568 potential properties to include and there might be different combinations with similar complexity.
569 The land geometry is of the utmost importance, but this choice is all but dictated by what mon-
570 soon is of interest: it is clear from previous literature that one must at least distinguish between
571 subtropical and tropical monsoons (Geen et al. 2020; Zhou and Xie 2018; Hui and Bordoni 2021).
572 As for how to represent the land surface, we agree that heat capacity is the most consequential of
573 the land characteristics, the zeroth order influence on the timing and the strength of the solstitial
574 circulations. Nevertheless, the TRACMIP experiments suggest that anything that affects surface
575 evaporation is also a fundamental knob, capable of shaping the regional circulation and the type
576 of monsoon regime that ensues. Interactive soil moisture (as in Chou et al. (2001)), or vegetation
577 (as, most crudely, in TRACMIP) both fit the bill; so do albedo, which determines the energy avail-
578 able to evaporation, and surface roughness, which alters wind and thus evaporation. The ways in
579 which these factors affect low-level MSE have not been investigated in the theoretical literature as
580 thoroughly as for heat capacity and continental geometry, and they deserve a deeper exploration.

581 The recent work by Smyth and Ming (2021), which investigates both albedo and soil moisture, is
582 a much welcome addition to the canon, but it is mostly limited to a simplified-physics GCM. We
583 suggest the need for more sensitivity experiments with full-physics comprehensive GCM in which
584 land's defining factors (surface roughness, albedo, soil moisture, and vegetation) can be explicitly
585 tuned for their effect on evaporation. This will allow a land model hierarchy to come into greater
586 focus, and we will be closer to the ideal where anyone who wants to study monsoon dynamics will
587 have a clearly defined array of tools from which to select the one best suited to their research.

588 *Acknowledgments.* Michela Biasutti, Aiko Voigt and the overall TRACMIP project were sup-
589 ported by the National Science Foundation under award # AGS-1565522. AV received support
590 from the German Ministry of Education and Research (BMBF) and FONA: Research for Sustain-
591 able Development (www.fona.de) under grant 01LK1509A. MB and SAH acknowledge support
592 from the Monsoon Mission Project under India's Ministry of Earth Sciences.

593 We thank Charles Blackmon-Luca for his help with data and software and Rick Rus-
594 sotto for ongoing discussions and his contribution to a previous version of this pa-
595 per. We especially thank the modeling groups responsible for the creation of TRACMIP
596 and of CMIP6. The model data used in this study are available in Google cloud
597 (<https://console.cloud.google.com/storage/browser/cmip6>), thanks to a grant to the Pangeo project
598 (<https://pangeo.io/>). Further information on TRACMIP, including sample scripts on how to access
599 its data via Pangeo, is provided at <https://gitlab.phaidra.org/voigta80/tracmip>.

600 **References**

601 Adam, O., T. Bischoff, and T. Schneider, 2016: Seasonal and interannual variations of the energy
602 flux equator and ITCZ. Part II: Zonally varying shifts of the ITCZ. *Journal of Climate*, **29** (9),
603 3219 – 3230, doi:10.1175/jcli-d-15-0512.1.

604 Arakawa, A., and W. H. Schubert, 1974: Interaction of a Cumulus Cloud Ensemble with the
605 Large-Scale Environment, Part I. *Journal of the Atmospheric Sciences*, **31** (3), 674–701, doi:
606 [https://doi.org/10.1175/1520-0469\(1974\)031<0674:IOACCE>2.0.CO;2](https://doi.org/10.1175/1520-0469(1974)031<0674:IOACCE>2.0.CO;2).

607 Back, L. E., and C. S. Bretherton, 2009: On the Relationship between SST Gradients, Boundary
608 Layer Winds, and Convergence over the Tropical Oceans. *Journal of Climate*, **22** (15), 4182 –
609 4196, doi:10.1175/2009jcli2392.1.

610 Biasutti, M., 2019: Rainfall trends in the African Sahel: Characteristics, processes, and causes.
611 *Wiley Interdisciplinary Reviews: Climate Change*, **10** (4), e591, doi:10.1002/wcc.591.

612 Biasutti, M., R. D. Russotto, A. Voigt, and C. C. Blackmon-Luca, 2021: The Effect of an Equato-
613 rial Continent on the Tropical Rain Belt. Part 1: Annual Mean Changes in the ITCZ. *Journal of*
614 *Climate*, **34** (14), 1–51, doi:10.1175/jcli-d-20-0739.1.

615 Biasutti, M., and Coauthors, 2018: Global energetics and local physics as drivers of past, present
616 and future monsoons. *Nature Geoscience*, **11** (6), 392 – 400, doi:10.1038/s41561-018-0137-1.

617 Bischoff, T., and T. Schneider, 2014: Energetic Constraints on the Position of the Intertropical
618 Convergence Zone. *Journal of Climate*, **27** (13), 4937 – 4951, doi:10.1175/jcli-d-13-00650.1.

619 Boos, W. R., and Z. Kuang, 2010: Dominant control of the South Asian monsoon by orographic
620 insulation versus plateau heating. *Nature*, **463** (7278), 218–222, doi:10.1038/nature08707.

621 Bordoni, S., and T. Schneider, 2008: Monsoons as eddy-mediated regime transitions of the tropical
622 overturning circulation. *Nature Geoscience*, **1** (8), 515 – 519, doi:10.1038/ngeo248.

623 Byrne, M. P., and T. Schneider, 2016: Narrowing of the ITCZ in a warming climate: Phys-
624 ical mechanisms. *Geophysical Research Letters*, **43** (21), 11,350 – 11,357, doi:10.1002/
625 2016gl070396.

- 626 Byrne, M. P., and L. Zanna, 2020: Radiative Effects of Clouds and Water Vapor on an Axisym-
627 metric Monsoon. *Journal of Climate*, **33** (20), 8789 – 8811, doi:10.1175/jcli-d-19-0974.1.
- 628 Charney, J. G., 1975: Dynamics of deserts and drought in the Sahel. *Quart. J. Roy. Meteor. Soc.*,
629 *101*, 193, **101**, 193 – 202.
- 630 Chiang, J., and C. M. Bitz, 2005: Influence of high latitude ice cover on the marine Intertropical
631 Convergence Zone. *Climate Dynamics*, **25** (5), 477 – 496.
- 632 Chou, C., and J. D. Neelin, 2003: Mechanisms Limiting the Northward Extent of the Northern
633 Summer Monsoons over North America, Asia, and Africa*. *Journal of Climate*, **16** (3), 406 –
634 425.
- 635 Chou, C., and J. D. Neelin, 2004: Mechanisms of Global Warming Impacts on Regional Trop-
636 ical Precipitation*. *Journal of Climate*, **17** (13), 2688 – 2701, doi:10.1175/1520-0442(2004)
637 017(2688:mogwio)2.0.co;2.
- 638 Chou, C., J. D. Neelin, and H. Su, 2001: Oceanatmosphereland feedbacks in an idealized mon-
639 soon. *Quarterly Journal of the Royal Meteorological Society*, **127** (576), 1869–1891, doi:
640 10.1002/qj.49712757602.
- 641 Dima, I. M., J. M. Wallace, and I. Kraucunas, 2005: Tropical Zonal Momentum Balance in the
642 NCEP Reanalyses. *Journal of the Atmospheric Sciences*, **62** (7), 2499 – 2513, doi:10.1175/
643 jas3486.1.
- 644 Emanuel, K., J. Neelin, and C. S. Bretherton, 1994: On large-scale circulations in convecting
645 atmospheres. *Q. J. R. Meteorol. Soc.*, **120**, 1111 – 1143.

646 Frierson, D. M. W., J. Lu, and G. Chen, 2007: Width of the Hadley cell in simple and
647 comprehensive general circulation models. *Geophysical Research Letters*, **34** (18), 224, doi:
648 10.1029/2007gl031115.

649 Gadgil, S., 2003: The Indian Monsoon and its Variability. *Annu. Rev. Earth Planet. Sci.*, **31** (1),
650 429 – 467, doi:10.1146/annurev.earth.31.100901.141251.

651 Geen, R., S. Bordoni, D. Battisti, and K. L. Hui, 2020: Monsoons, ITCZs, and the Concept of the
652 Global Monsoon. *Reviews of Geophysics*, **58** (4), doi:10.1029/2020rg000700.

653 Geen, R., F. H. Lambert, and G. K. Vallis, 2019: Processes and Timescales in Onset and
654 Withdrawal of Aquaplanet Monsoons. *J. Atmos. Sci.*, **76** (8), 2357 – 2373, doi:10.1175/
655 jas-d-18-0214.1.

656 Gill, A. E., 1980: Some simple solutions for heatinduced tropical circulation. *Quarterly Journal*
657 *of the Royal Meteorological Society*, **106** (449), 447 – 462, doi:10.1002/qj.49710644905.

658 Hill, S. A., 2019: Theories for Past and Future Monsoon Rainfall Changes. *Current Climate*
659 *Change Reports*, **5** (3), 1 – 12, doi:10.1007/s40641-019-00137-8.

660 Hill, S. A., Y. Ming, I. M. Held, and M. Zhao, 2017: A Moist Static Energy BudgetBased Analysis
661 of the Sahel Rainfall Response to Uniform Oceanic Warming. *Journal of Climate*, **30** (15), 5637
662 – 5660, doi:10.1175/jcli-d-16-0785.1.

663 Hui, K. L., and S. Bordoni, 2021: Response of Monsoon Rainfall to Changes in the Latitude of the
664 Equatorward Coastline of a Zonally Symmetric Continent. *J. Atmos. Sci.*, **78** (5), 1429 – 1444,
665 doi:10.1175/jas-d-20-0110.1.

666 Hurley, J. V., and W. R. Boos, 2013: Interannual Variability of Monsoon Precipitation and Local
667 Subcloud Equivalent Potential Temperature. *Journal of Climate*, **26** (23), 9507–9527, doi:10.
668 1175/jcli-d-12-00229.1.

669 Jeevanjee, N., P. Hassanzadeh, S. Hill, and A. Sheshadri, 2017: A perspective on climate model
670 hierarchies. *Journal of Advances in Modeling Earth Systems*, **9** (4), 1760–1771, doi:10.1002/
671 2017MS001038.

672 Kang, S. M., D. M. W. Frierson, and I. M. Held, 2009: The Tropical Response to Extrat-
673 ropical Thermal Forcing in an Idealized GCM: The Importance of Radiative Feedbacks and
674 Convective Parameterization. *Journal of the Atmospheric Sciences*, **66** (9), 2812 – 2827, doi:
675 10.1175/2009jas2924.1.

676 Kang, S. M., I. M. Held, D. M. W. Frierson, and M. Zhao, 2008: The Response of the ITCZ
677 to Extratropical Thermal Forcing: Idealized Slab-Ocean Experiments with a GCM. *Journal of*
678 *Climate*, **21** (14), 3521 – 3532, doi:10.1175/2007jcli2146.1.

679 Kuang, Z., 2010: Linear Response Functions of a Cumulus Ensemble to Temperature and Moisture
680 Perturbations and Implications for the Dynamics of Convectively Coupled Waves. *Journal of the*
681 *Atmospheric Sciences*, **67** (4), 941–962, doi:10.1175/2009jas3260.1.

682 Lindzen, R., and S. Nigam, 1987: On the role of sea-surface temperature-gradients in forcing
683 low-level winds and convergence in the tropics. *J. Atmos. Sci.*, **44**, 2418 – 2436.

684 Maroon, E. A., and D. M. W. Frierson, 2016: The impact of a continent’s longitudinal extent on
685 tropical precipitation. *Geophysical Research Letters*, **43** (22), 11,921 – 11,929, doi:10.1002/
686 2016gl071518.

- 687 Maroon, E. A., D. M. W. Frierson, S. M. Kang, and J. Scheff, 2016: The Precipitation Response
688 to an Idealized Subtropical Continent. *Journal of Climate*, **29** (12), 4543 – 4564, doi:10.1175/
689 jcli-d-15-0616.1.
- 690 Neelin, J. D., and N. Zeng, 2000: A Quasi-Equilibrium Tropical Circulation Model Formula-
691 tion*. *Journal of the Atmospheric Sciences*, **57** (11), 1741–1766, doi:10.1175/1520-0469(2000)
692 057<1741:aqetcm>2.0.co;2.
- 693 Nicholson, S. E., 2018: The ITCZ and the Seasonal Cycle over Equatorial Africa. *Bulletin of the*
694 *American Meteorological Society*, **99** (2), 337 – 348, doi:10.1175/bams-d-16-0287.1.
- 695 Nie, J., W. R. Boos, and Z. Kuang, 2010: Observational Evaluation of a Convective Quasi-
696 Equilibrium View of Monsoons. *Journal of Climate*, **23** (16), 4416 – 4428, doi:10.1175/
697 2010jcli3505.1.
- 698 Peterson, H. G., and W. Boos, 2020: Feedbacks and eddy diffusivity in an energy balance
699 model of tropical rainfall shifts. *npj Climate and Atmospheric Sciences*, **3** (11), doi:10.1038/
700 s41612-020-0114-4.
- 701 Priv, N. C., and R. A. Plumb, 2007: Monsoon Dynamics with Interactive Forcing. Part I: Axisym-
702 metric Studies. *J. Atmos. Sci.*, **64** (5), 1417 – 1430, doi:10.1175/jas3916.1.
- 703 Ramage, C. S., 1971: *Monsoon Meteorology*. Academic Press, Academic Press.
- 704 Raymond, D., 1995: Regulation of Moist Convection over the West Pacific Warm Pool. *Journal*
705 *of Atmospheric Sciences*, **52**, 3945 – 3959.
- 706 Raymond, D., S. Sessions, A. H. Sobel, and Z. Fuchs, 2009: The mechanics of gross moist stabil-
707 ity. *J. Adv. Model. Earth Syst*, **1** (9), 1 – 20, doi:DOI:10.3894/JAMES.2009.1.9.

708 Rodwell, M. J., and B. J. Hoskins, 1996: Monsoons and the dynamics of deserts. *Quarterly Jour-*
709 *nal of the Royal Meteorological Society*, **122 (534)**, 1385–1404, doi:10.1002/qj.49712253408.

710 Rcz, Z., and R. K. Smith, 1999: The dynamics of heat lows. *Quarterly Journal of the Royal*
711 *Meteorological Society*, **125 (553)**, 225 – 252.

712 Schneider, T., T. Bischoff, and G. H. Haug, 2014: Migrations and dynamics of the intertropical
713 convergence zone. *Nature*, **513 (7516)**, 45 – 53, doi:doi:10.1038/nature13636.

714 Shaw, T. A., A. Voigt, S. M. Kang, and J. Seo, 2015: Response of the intertropical convergence
715 zone to zonally asymmetric subtropical surface forcings. *Geophysical Research Letters*, **42 (22)**,
716 9961 – 9969, doi:10.1002/2015gl066027.

717 Shekhar, R., and W. R. Boos, 2017: Weakening and Shifting of the Saharan Shallow Meridional
718 Circulation during Wet Years of the West African Monsoon. *Journal of Climate*, **30 (18)**, 7399–
719 7422, doi:10.1175/jcli-d-16-0696.1, 1609.08515.

720 Singh, M. S., 2019: Limits on the Extent of the Solstitial Hadley Cell: The Role of Planetary
721 Rotation. *J. Atmos. Sci.*, **76 (7)**, 1989 – 2004, doi:10.1175/jas-d-18-0341.1.

722 Smyth, J. E., and Y. Ming, 2021: Investigating the impact of land surface characteristics on mon-
723 soon dynamics with idealized model simulations and theories. *Journal of Climate*, 1–49, doi:
724 10.1175/jcli-d-20-0954.1.

725 Sobel, A. H., and C. S. Bretherton, 2000: Modeling tropical precipitation in a single column.
726 *Journal of Climate*, **13**, 4378 – 4392.

727 Sobel, A. H., and J. Neelin, 2006: The boundary layer contribution to intertropical convergence
728 zones in the quasi-equilibrium tropical circulation model framework. *Theoretical and Compu-*
729 *tational Fluid Dynamics*, **20 (5)**, 323 – 350.

730 Sultan, B., and S. Janicot, 2003: The West African Monsoon Dynamics. Part II: The Preonset
731 and Onset of the Summer Monsoon. *Journal of Climate*, **16 (21)**, 3407–3427, doi:10.1175/
732 1520-0442(2003)016(3407:twamdp)2.0.co;2.

733 Tulich, S. N., and B. E. Mapes, 2010: Transient Environmental Sensitivities of Explicitly
734 Simulated Tropical Convection. *Journal of the Atmospheric Sciences*, **67 (4)**, 923–940, doi:
735 10.1175/2009jas3277.1.

736 Voigt, A., N. Albern, P. Ceppi, K. Grise, Y. Li, and B. Medeiros, 2021: Clouds, radiation, and
737 atmospheric circulation in the present-day climate and under climate change. *Wiley Interdisci-*
738 *plinary Reviews: Climate Change*, **12 (2)**, e694, doi:10.1002/wcc.694.

739 Voigt, A., S. Bony, J.-L. Dufresne, and B. Stevens, 2014: The radiative impact of clouds on the
740 shift of the Intertropical Convergence Zone. *Geophysical Research Letters*, **41 (12)**, 4308 –
741 4315, doi:10.1002/2014gl060354.

742 Voigt, A., and Coauthors, 2016: The tropical rain belts with an annual cycle and a continent
743 model intercomparison project: TRACMIP. *J. Adv. Model. Earth Syst*, **8 (4)**, 1868 – 1891,
744 doi:10.1002/2016ms000748.

745 Wang, B., and Q. Ding, 2008: Global monsoon: Dominant mode of annual variation in the tropics.
746 *Dynamics of Atmospheres and Oceans*, **44 (3-4)**, 165 – 183, doi:10.1016/j.dynatmoce.2007.05.
747 002.

748 Webster, P., V. O. Magana, and T. N. Palmer, 1998: Monsoons: Processes, predictability, and the
749 prospects for prediction. *Journal of Geophysical Research-Oceans*, **103 (C7)**, 14 451 – 14 510,
750 doi:10.1029/97jc02719.

- 751 Wei, H. H., and S. Bordoni, 2018: Energetic Constraints on the ITCZ Position in Idealized Simu-
752 lations With a Seasonal Cycle. *Journal of Advances in Modeling Earth Systems*, **10** (7), 1708 –
753 1725, doi:10.1029/2018ms001313.
- 754 Zhai, J., and W. R. Boos, 2017: The drying tendency of shallow meridional circulations in mon-
755 soons. *Quarterly Journal of the Royal Meteorological Society*, **143** (708), 2655 – 2664, doi:
756 10.1002/qj.3091.
- 757 Zhang, Y., and S. Fueglistaler, 2020: How Tropical Convection Couples High Moist Static Energy
758 Over Land and Ocean. *Geophysical Research Letters*, **47** (2), 186, doi:10.1029/2019gl086387.
- 759 Zhou, W., and S.-P. Xie, 2018: A Hierarchy of Idealized Monsoons in an Intermediate GCM.
760 *Journal of Climate*, **31** (22), 9021 – 9036, doi:10.1175/jcli-d-18-0084.1.

761 **LIST OF TABLES**

762 **Table 1.** List of atmospheric GCMs used in this study, along with the coupled Earth
763 System model that each atmospheric model is a component of, if applicable.
764 Only the models following protocol (not starred) are included in the multi-
765 model means. All models except CaltechGray are full physics GCMs. Citations
766 and additional details such as model resolution are listed in Voigt et al. (2016). . . . 37

Atmospheric model	Component of	Protocol
CaltechGray	N/A	yes
CAM3	CCSM3	yes
CAM4	CCSM4	yes
CAM5Nor	NorESM2	yes
CNRM-AM5	CNRM-CM5	yes
ECHAM6.1	MPI-ESM	yes
MetUM-CTL*	GA6.0	no: heat capacity as in AquaControl
MetUM-ENT*	GA6.0 (modified)	no: heat capacity as in AquaControl
MIROC5 (atmospheric component)	MIROC5	yes
MPAS (atmospheric component)	MPAS	yes

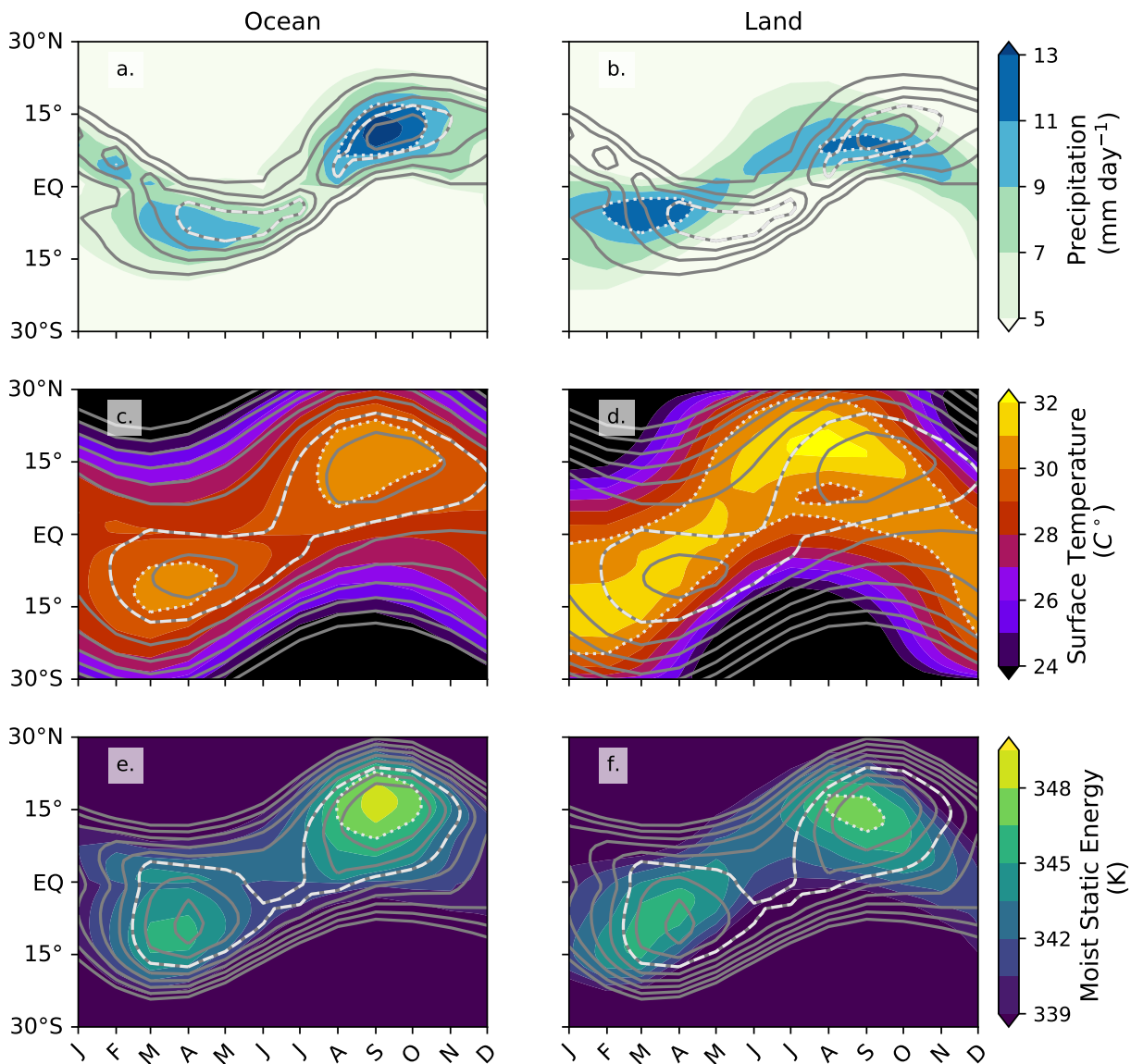
767 TABLE 1. List of atmospheric GCMs used in this study, along with the coupled Earth System model that
768 each atmospheric model is a component of, if applicable. Only the models following protocol (not starred)
769 are included in the multi-model means. All models except CaltechGray are full physics GCMs. Citations and
770 additional details such as model resolution are listed in Voigt et al. (2016).

771 **LIST OF FIGURES**

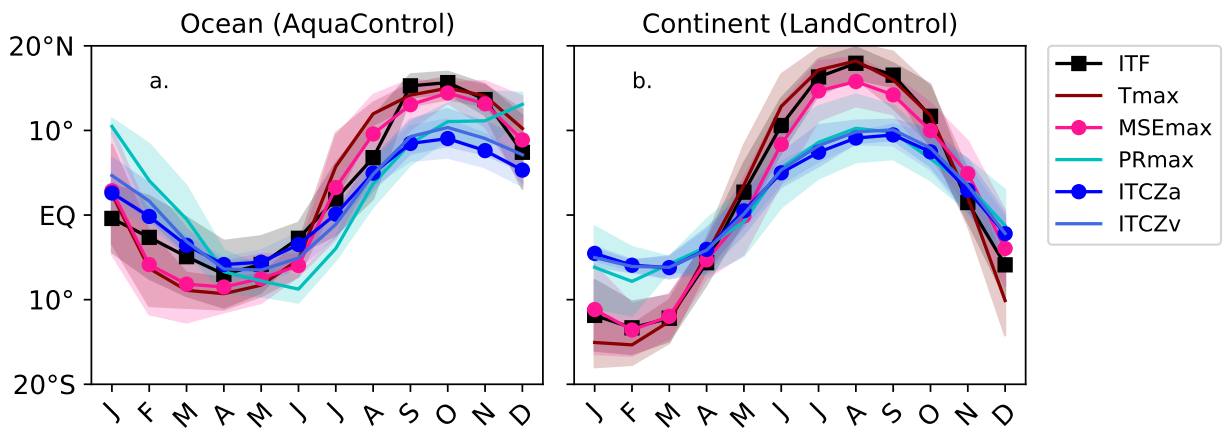
- 772 **Fig. 1.** Latitude-Month Hovmöller diagram of the climatological ocean (left: a,c,e) and continent
773 (right: b,d,f) sector mean of the LandControl precipitation (a,b), surface temperature (c,d),
774 low-level MSE (e,f). The AquaControl fields are repeated as contours superimposed on the
775 LandControl shading for reference. In all panels, the same contour level is dashed in the
776 AquaControl and dotted in the LandControl to facilitate the comparison of the timing and
777 intensity of the maxima in each field (refer to the colorbar to identify the values correspond-
778 ing to the highlighted contours). 41
- 779 **Fig. 2.** Meridional positions, as a function of climatological month, of the ITCZ (ITCZ_a and ITCZ_v
780 indicate the definitions of Adam et al (2016) and Voigt et al (2014), respectively; blue lines),
781 the maximum in rainfall (light blue), the minimum in SLP (indicated as the InterTropical
782 Front, ITF, black), the maximum in low-level MSE (magenta), and the maximum in surface
783 temperature (red). Left panel (a) is for the ensemble and zonal mean of the AquaControl
784 simulations, right panel (b) is for the ensemble and continent sector mean of the LandControl
785 simulations. Shading indicates one standard deviation in the multi-model ensemble. 42
- 786 **Fig. 3.** Top (a,b): Position of the ITCZ in the AquaControl (solid lines) and LandControl (dashed
787 lines) according to the definition of Adam et al (2016, a) and Voigt et al (2014, b) as cal-
788 culated from smoothed daily data. Bottom (c,d): the speed of meridional migration of the
789 ITCZ (according to the Adam et al. (2016) definition) in the AquaControl (c, solid lines)
790 and in the LandControl (d, dashed lines). The perfect ellipses in c and d are obtained by
791 fitting the ITCZ position with two Fourier components (time mean plus a single annual si-
792 nusoid) and plotting the corresponding position and velocity. Migration speeds outside the
793 ellipses correspond to rapid transitions. Individual models are color-coded (see Figure 4 for
794 a legend), the multi-model mean is given by the thick black lines. 43
- 795 **Fig. 4.** Width of the ITCZ as indicated by the zero contour of the P-E field. The left panel is for the
796 zonal mean of the AquaControl simulations; the middle panel is for the sector mean of the
797 LandControl simulations. The right panel indicates the meridional span of the ITCZ in its
798 seasonal march (the southernmost reach of the southern zero P-E contour and the northern-
799 most reach of the northern zero P-E contour); broad bars for the LandControl case and thin
800 lines for the AquaControl case; y-axis on the left, corresponding to that on the other panels.
801 The right y-axis measures the maximum width of the ITCZ (distance between the southern
802 and northern zero P-E contours) during the course of the year for the AquaControl zonal
803 mean rain band (dots) and the LandControl sector mean continental rain band (squares).
804 Individual models are color-coded as indicated in the right panel, the multi-model mean is
805 given by the thick black lines. 44
- 806 **Fig. 5.** Spatial extent of the summer rain bands (top) and loci of seasonal wind reversal (bottom). a:
807 Map of the LandControl global monsoon, as defined by a precipitation criterion. Each model
808 is color-coded as indicated in the right-hand panel and the multi-model mean is indicated
809 in black. b: maximum meridional summer extent of the rain-defined global monsoon domain
810 in each model (bars are for the LandControl case and thin lines are for the AquaControl case)
811 and in the multi-model mean. c. Map of the LandControl global monsoon, as defined by a
812 wind reversal criterion. Each model is color-coded and the multi-model mean is hatched in
813 black. d: as in b, but for the wind-reversal criterion. Refer to the text for the exact definition
814 of the rainfall and wind criteria for the global monsoon in the Land and Aqua cases. 45
- 815 **Fig. 6.** Maps of the surface temperature (shaded) and precipitation (black contours, every 2mm
816 day⁻¹, skipping the zero contour) LandControl minus AquaControl ensemble-mean sea-
817 sonal anomalies. The seasonal means are DJF (a), MAM (b), JJA (c) and SON (d). The

818	position of the AquaControl rain band for each season (as indicated by the 6mm day ⁻¹	
819	contour) is superimposed in grey for reference.	46
820	Fig. 7. Top (a): summertime (JJA in the NH and DJF in the SH) ensemble mean LandControl minus AquaControl ensemble-mean anomalies in 300hPa temperature (shaded) and in 700hPa geopotential (contours, contour interval is 8m; dashed lines indicate negative anomalies, the zero contour is omitted), and 700hPa LandControl full wind field (vectors; only wind speeds greater than 3m/s are plotted; see reference arrow on the left). Summertime rainfall anomalies less than -2mm day ⁻¹ are shaded in brown and those greater than 2 (4) are shaded in green (dark green); Bottom (b): Same as in (a), but shading indicates 925hPa geopotential heights; contours indicate precipitable water (contour interval is 5g Kg ⁻¹); and wind vectors are for the 925hPa anomalies (only wind speeds larger than 1m/s are plotted, see reference arrow on the left).	47
830	Fig. 8. Maps of NH summertime (JJA) LandControl minus AquaControl ensemble-mean anomalous MSE transport at 925hPa (left: a,c,e,g,i) and 300hPa (right: b,d,f,h,l). The total advection anomalies are given in the top panels (a,b). The other panels show: (c,d) the advection of the anomalous MSE gradient by the basic-state zonal wind; (e,f) the advection of the basic-state MSE gradient by the anomalous zonal wind; (g,h) the advection of the anomalous MSE gradient by the basic-state meridional wind; and (i,l) the advection of the basic-state MSE gradient by the anomalous meridional wind. Units are in °C m s ⁻¹ (lat/lon degree) ⁻¹	48
837	Fig. 9. Vertical average profile of summertime (JJA in the NH and DJF in the SH) LandControl minus AquaControl ensemble-mean anomalous MSE transport in the western subtropical corners of the TRACMIP continent. The total advection anomalies are given in black (the sum of the linearized terms is given in the dashed black line). Blu refers to the advection by the mean wind of the anomalous MSE, magenta refers the advection by the anomalous wind of the mean MSE. Dotted lines refer to zonal terms and dash-dotted lines to meridional terms. The dominant terms are indicated in the legend and are plotted with a shading corresponding to plus or minus one standard deviation in the multi-model ensemble. The vertical axis is pressure in hPa; the MSE transport terms are calculated in units of °C m s ⁻¹ (lat/lon degree) ⁻¹	49
847	Fig. 10. Latitude/time Hovmöller diagram of climatological LandControl minus AquaControl multi-model-mean monthly anomalies in (a,d) rainfall in mm day ⁻¹ (b,d) frequency of rainy days in percentage, and (c,f) simple daily intensity index in mm day ⁻¹ . Superimposed on the shaded fields are (a,d) the AquaControl climatological rainfall (gray contours) and (b,c,e,f) the LandControl-AquaControl monthly rainfall anomalies (contours colored according to the colorbar in a). Top (a,b,c) is for the mean of the models with reduced heat capacity over land. Bottom (d,e,f) is for the average of the models with unchanged heat capacity.	50
854	Fig. 11. The annual cycle of LandControl minus AquaControl rainfall anomalies averaged zonally (LandControl data over the continental sector only) and over (a) 10°15° N and (b) 10°15° S . The solid thin colored lines are individual models that followed protocol, the thick solid black line is their multi-model mean, and the light shading indicates a spread of ± 1 standard deviation. The dash-dotted lines are the two models that did not reduce heat capacity in the continental area.	51
860	Fig. 12. The effect of heat capacity on ascent profiles. (a) Vertical velocity omega profiles during SH summer in LandControl (DJF, shaded, averaged over the continental sector) and AquaControl (MAM contours, zonally averaged). Fields are the multi-model mean of the models that followed the full TRACMIP protocol in setting up land points. (b) Vertical velocity omega profiles during SH summer (as in a) but averaged over the latitude of tropical ascent and	

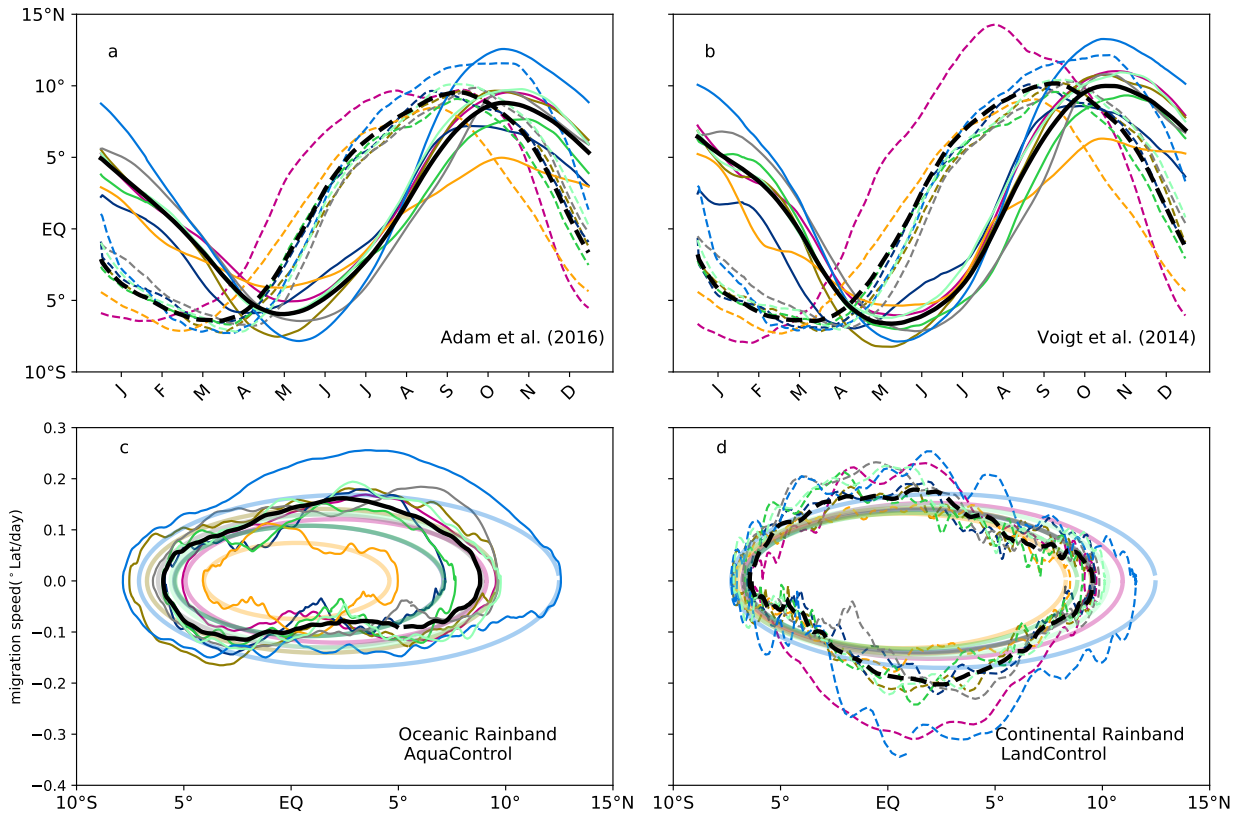
865 plotted for each individual model (solid for LandControl and dashed for AquaControl; note
866 that we plot negative values both right and left of the vertical zero line, to allow for a cleaner
867 comparison of the profile shape in LandControl (left) and AquaControl (right). (c) and (d):
868 As in (a) and (b), but for the average of the two MetUM models, which did not reduce land's
869 heat capacity. Southern Hemisphere summer season is therefore defined as MAM for both
870 LandControl and AquaControl. 52



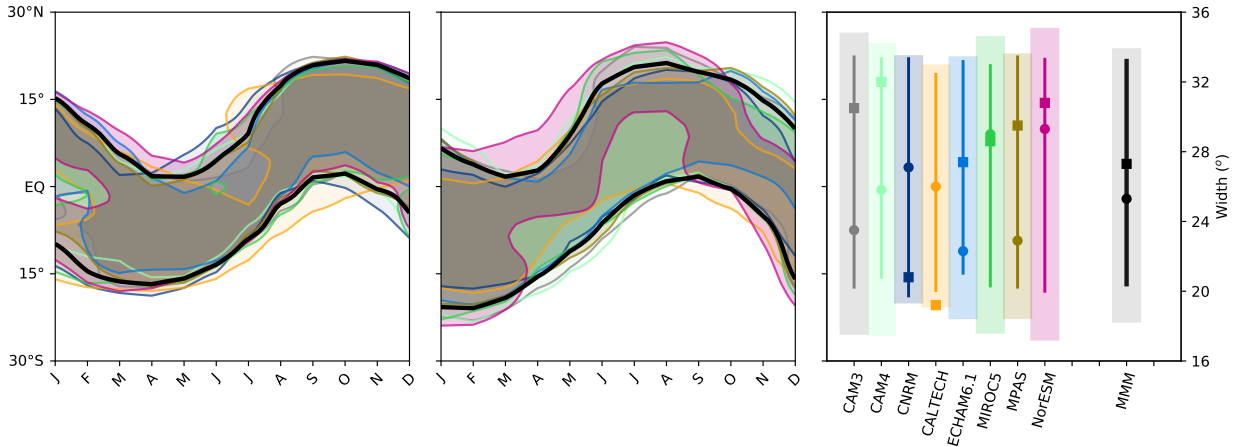
871 FIG. 1. Latitude-Month Hovmöeller diagram of the climatological ocean (left: a,c,e) and continent (right:
 872 b,d,f) sector mean of the LandControl precipitation (a,b), surface temperature (c,d), low-level MSE (e,f). The
 873 AquaControl fields are repeated as contours superimposed on the LandControl shading for reference. In all
 874 panels, the same contour level is dashed in the AquaControl and dotted in the LandControl to facilitate the
 875 comparison of the timing and intensity of the maxima in each field (refer to the colorbar to identify the values
 876 corresponding to the highlighted contours).



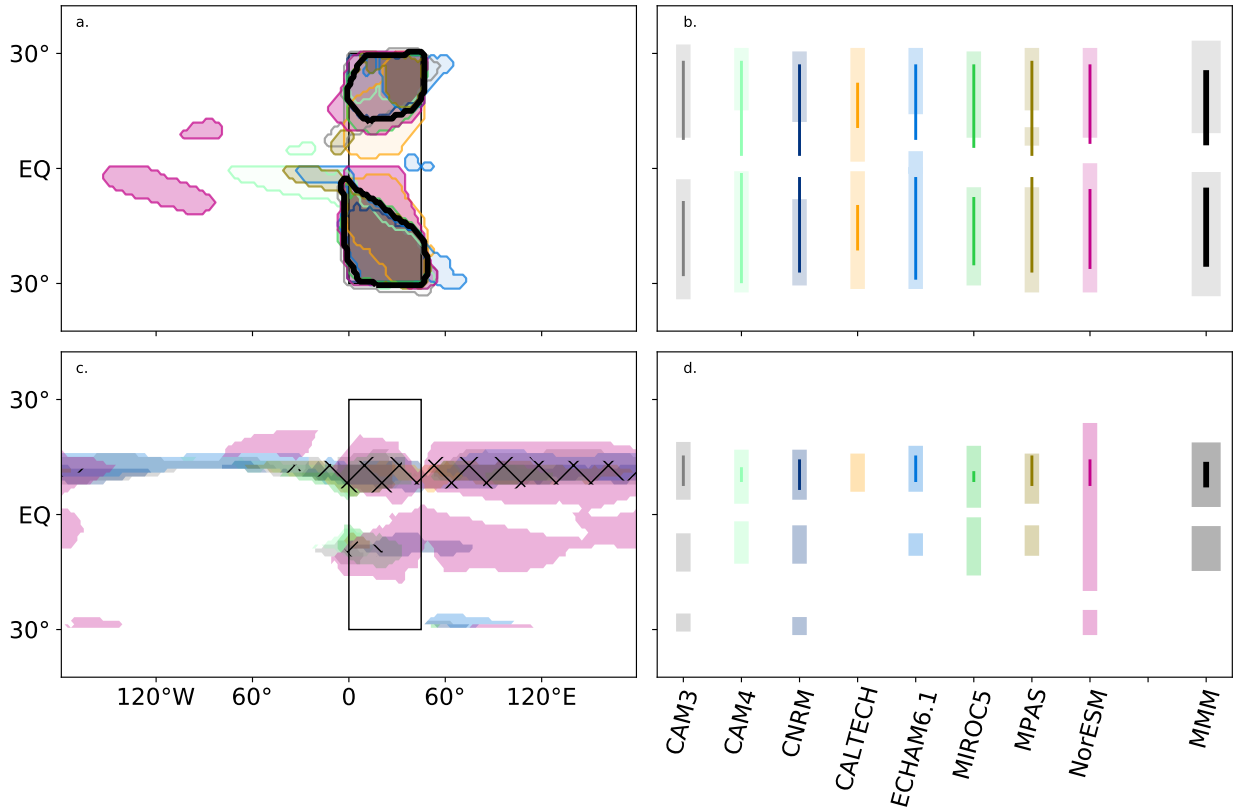
877 FIG. 2. Meridional positions, as a function of climatological month, of the ITCZ (ITCZa and ITCZv indicate
 878 the definitions of Adam et al (2016) and Voigt et al (2014), respectively; blue lines), the maximum in rainfall
 879 (light blue), the minimum in SLP (indicated as the InterTropical Front, ITF, black), the maximum in low-level
 880 MSE (magenta), and the maximum in surface temperature (red). Left panel (a) is for the ensemble and zonal
 881 mean of the AquaControl simulations, right panel (b) is for the ensemble and continent sector mean of the
 882 LandControl simulations. Shading indicates one standard deviation in the multi-model ensemble.



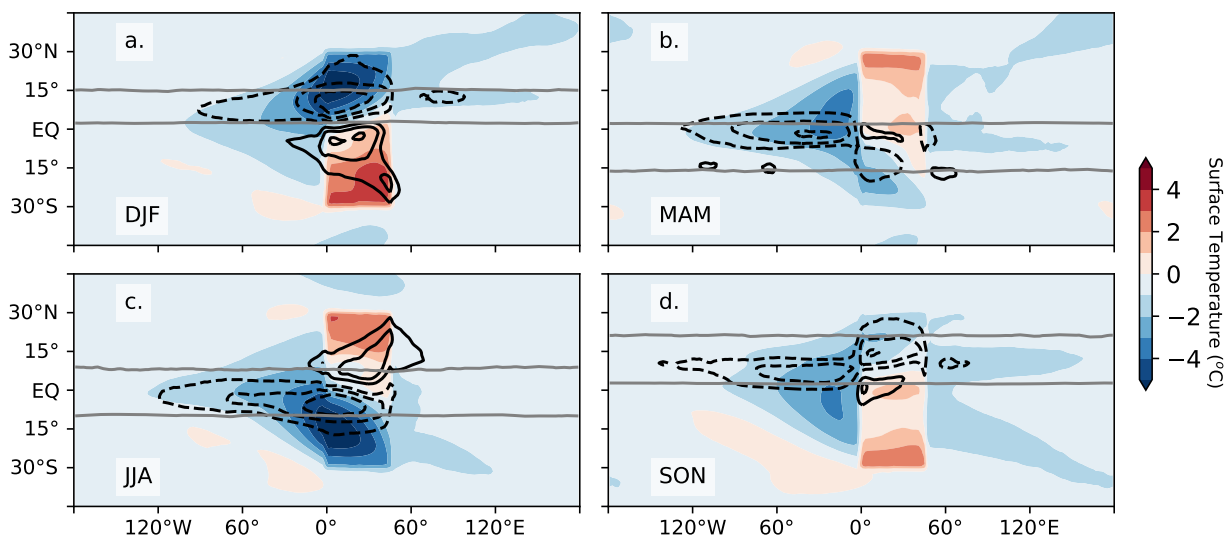
883 FIG. 3. Top (a,b): Position of the ITCZ in the AquaControl (solid lines) and LandControl (dashed lines)
 884 according to the definition of Adam et al (2016, a) and Voigt et al (2014, b) as calculated from smoothed
 885 daily data. Bottom (c,d): the speed of meridional migration of the ITCZ (according to the Adam et al. (2016)
 886 definition) in the AquaControl (c, solid lines) and in the LandControl (d, dashed lines). The perfect ellipses in
 887 c and d are obtained by fitting the ITCZ position with two Fourier components (time mean plus a single annual
 888 sinusoid) and plotting the corresponding position and velocity. Migration speeds outside the ellipses correspond
 889 to rapid transitions. Individual models are color-coded (see Figure 4 for a legend), the multi-model mean is
 890 given by the thick black lines.



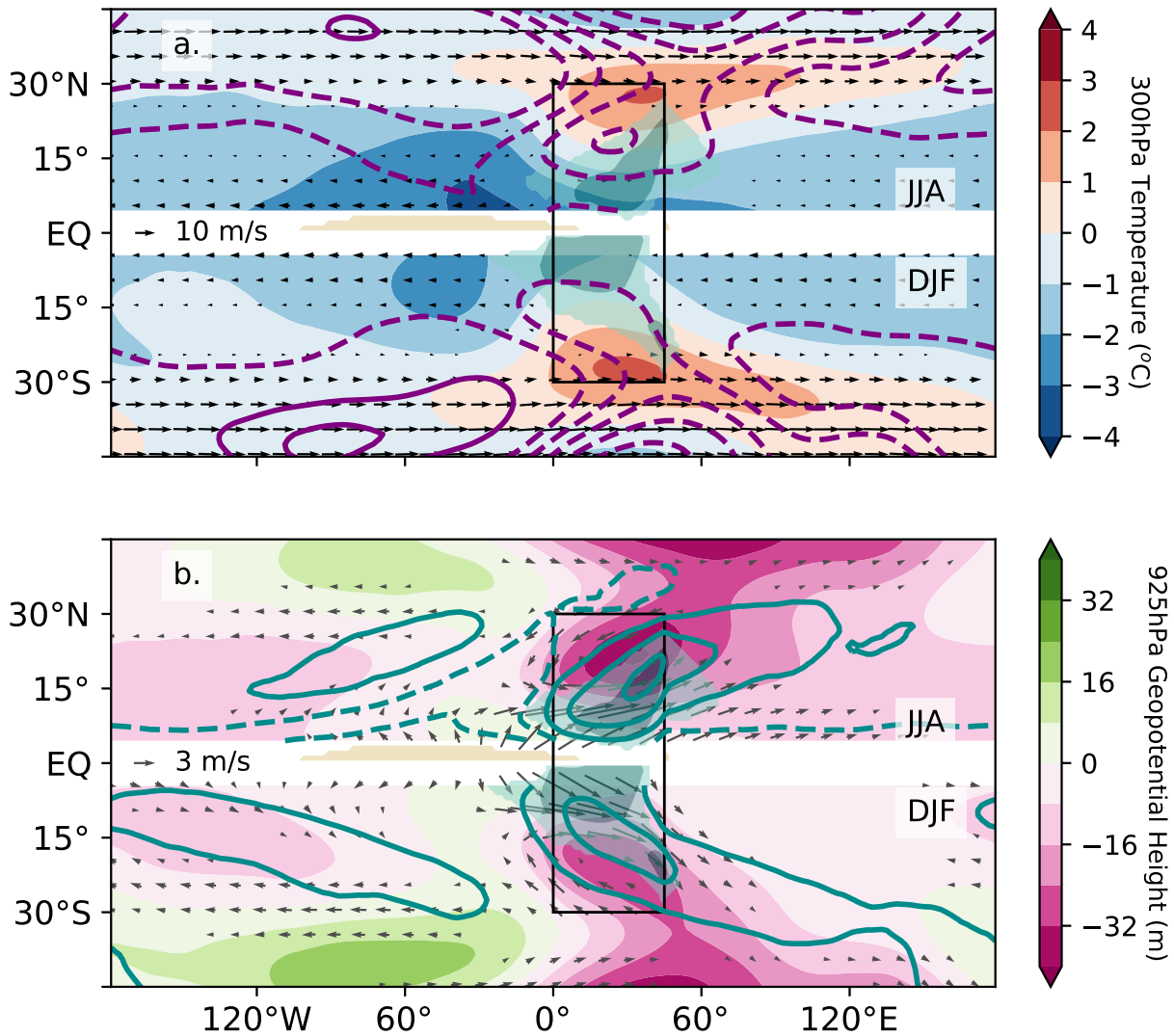
891 FIG. 4. Width of the ITCZ as indicated by the zero contour of the P-E field. The left panel is for the zonal
 892 mean of the AquaControl simulations; the middle panel is for the sector mean of the LandControl simulations.
 893 The right panel indicates the meridional span of the ITCZ in its seasonal march (the southernmost reach of
 894 the southern zero P-E contour and the northernmost reach of the northern zero P-E contour); broad bars for
 895 the LandControl case and thin lines for the AquaControl case; y-axis on the left, corresponding to that on the
 896 other panels. The right y-axis measures the maximum width of the ITCZ (distance between the southern and
 897 northern zero P-E contours) during the course of the year for the AquaControl zonal mean rain band (dots) and
 898 the LandControl sector mean continental rain band (squares). Individual models are color-coded as indicated in
 899 the right panel, the multi-model mean is given by the thick black lines.



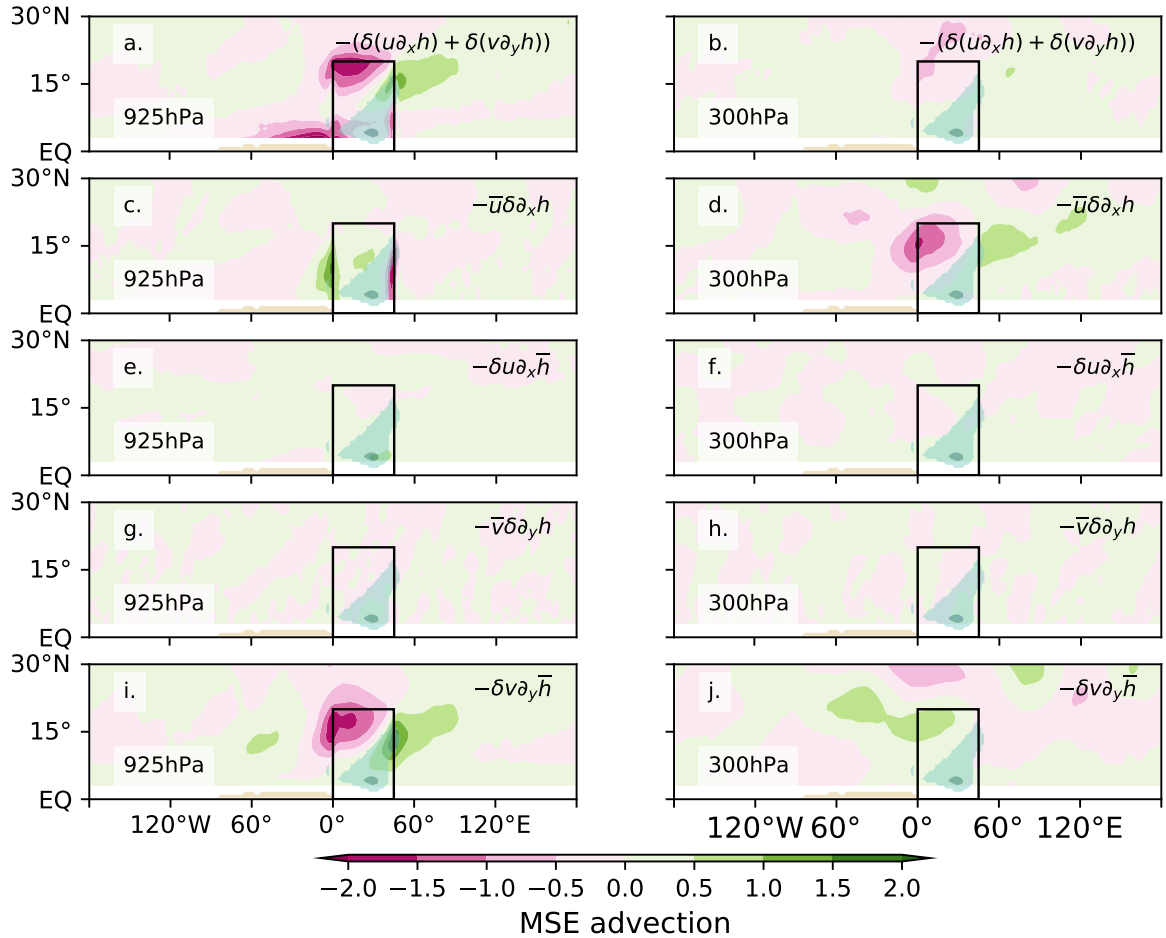
900 FIG. 5. Spatial extent of the summer rain bands (top) and loci of seasonal wind reversal (bottom). a: Map of
 901 the LandControl global monsoon, as defined by a precipitation criterion. Each model is color-coded as indicated
 902 in the right-hand panel and the multi-model mean is indicated in black. b: maximum meridional summer extent
 903 of the rain-defined global monsoon domain in each model (bars are for the LandControl case and thin lines are
 904 for the AquaControl case) and in the multi-model mean. c. Map of the LandControl global monsoon, as defined
 905 by a wind reversal criterion. Each model is color-coded and the multi-model mean is hatched in black. d: as in
 906 b, but for the wind-reversal criterion. Refer to the text for the exact definition of the rainfall and wind criteria for
 907 the global monsoon in the Land and Aqua cases.



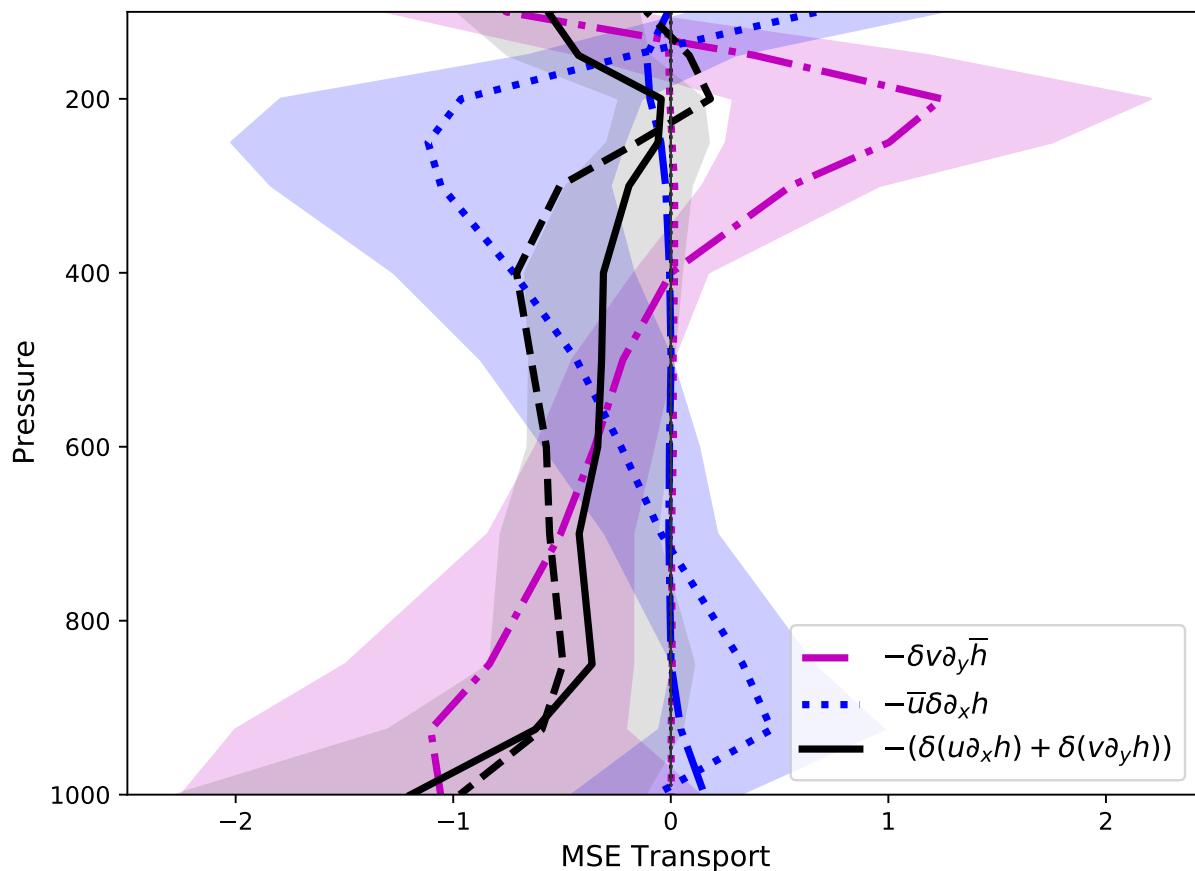
908 FIG. 6. Maps of the surface temperature (shaded) and precipitation (black contours, every 2mm day^{-1} ,
 909 skipping the zero contour) LandControl minus AquaControl ensemble-mean seasonal anomalies. The seasonal
 910 means are DJF (a), MAM (b), JJA (c) and SON (d). The position of the AquaControl rain band for each season
 911 (as indicated by the 6mm day^{-1} contour) is superimposed in grey for reference.



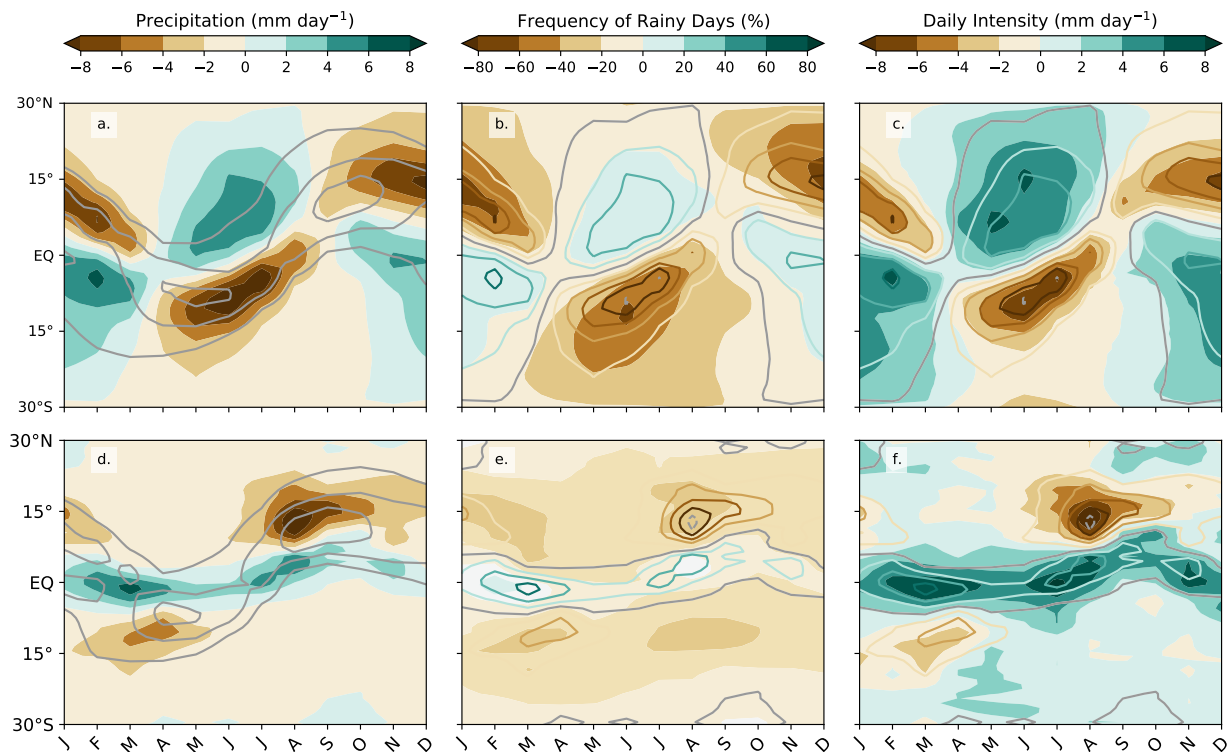
912 FIG. 7. Top (a): summertime (JJA in the NH and DJF in the SH) ensemble mean LandControl minus Aqua-
 913 Control ensemble-mean anomalies in 300hPa temperature (shaded) and in 700hPa geopotential (contours, con-
 914 tour interval is 8m; dashed lines indicate negative anomalies, the zero contour is omitted), and 700hPa Land-
 915 Control full wind field (vectors; only wind speeds greater than 3m/s are plotted; see reference arrow on the
 916 left). Summertime rainfall anomalies less than -2mm day^{-1} are shaded in brown and those greater than 2 (4) are
 917 shaded in green (dark green); Bottom (b): Same as in (a), but shading indicates 925hPa geopotential heights;
 918 contours indicate precipitable water (contour interval is 5g Kg^{-1}); and wind vectors are for the 925hPa anomalies
 919 (only wind speeds larger than 1m/s are plotted, see reference arrow on the left).



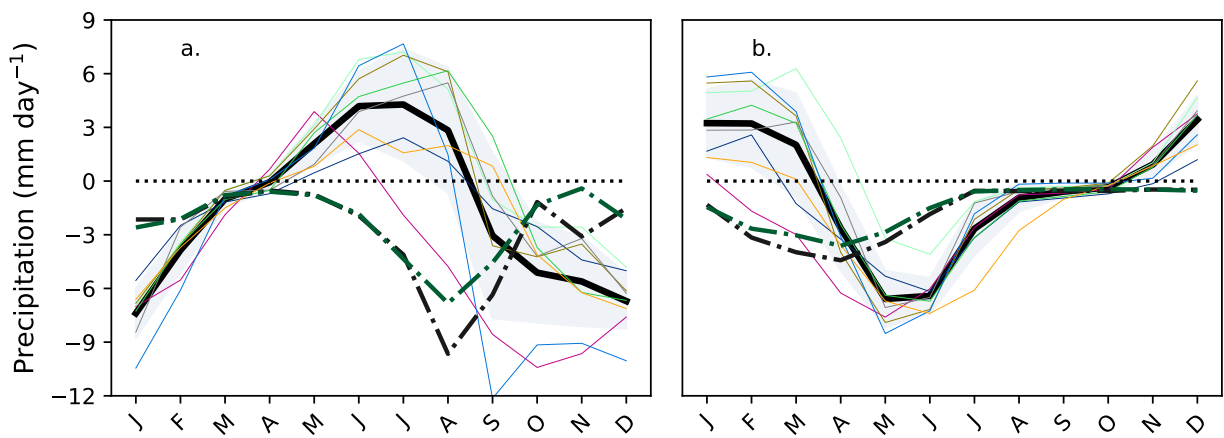
920 FIG. 8. Maps of NH summertime (JJA) LandControl minus AquaControl ensemble-mean anomalous MSE
 921 transport at 925hPa (left: a,c,e,g,i) and 300hPa (right: b,d,f,h,l). The total advection anomalies are given in the
 922 top panels (a,b). The other panels show: (c,d) the advection of the anomalous MSE gradient by the basic-state
 923 zonal wind; (e,f) the advection of the basic-state MSE gradient by the anomalous zonal wind; (g,h) the advection
 924 of the anomalous MSE gradient by the basic-state meridional wind; and (i,l) the advection of the basic-state MSE
 925 gradient by the anomalous meridional wind. Units are in $^{\circ}\text{C m s}^{-1} (\text{lat/lon degree})^{-1}$.



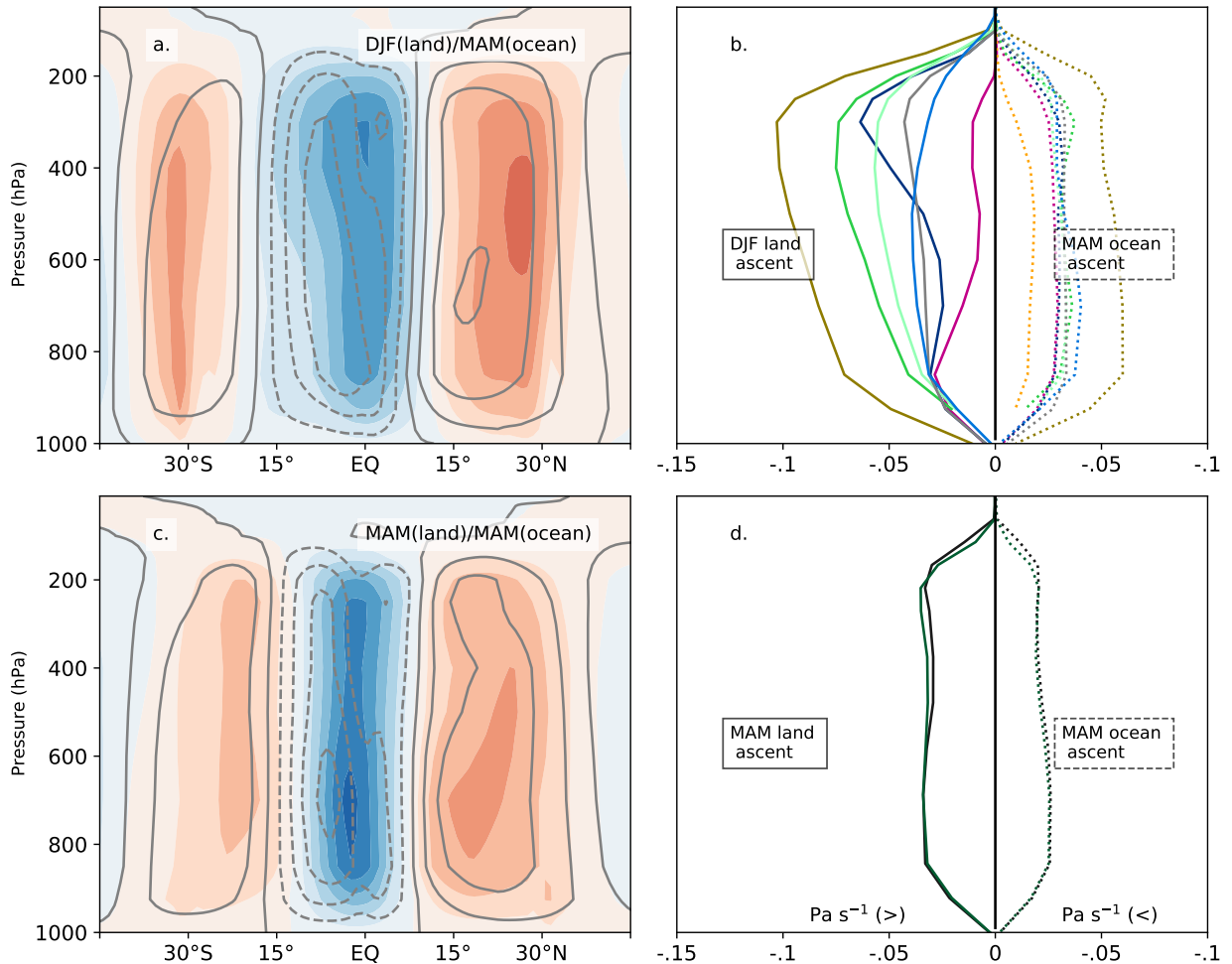
926 FIG. 9. Vertical average profile of summertime (JJA in the NH and DJF in the SH) LandControl minus
 927 AquaControl ensemble-mean anomalous MSE transport in the western subtropical corners of the TRACMIP
 928 continent. The total advection anomalies are given in black (the sum of the linearized terms is given in the
 929 dashed black line). Blu refers to the advection by the mean wind of the anomalous MSE, magenta refers the
 930 advection by the anomalous wind of the mean MSE. Dotted lines refer to zonal terms and dash-dotted lines to
 931 meridional terms. The dominant terms are indicated in the legend and are plotted with a shading corresponding
 932 to plus or minus one standard deviation in the multi-model ensemble. The vertical axis is pressure in hPa; the
 933 MSE transport terms are calculated in units of $^{\circ}\text{C m s}^{-1} (\text{lat/lon degree})^{-1}$.



934 FIG. 10. Latitude/time Hovmoeller diagram of climatological LandControl minus AquaControl multi-model-
 935 mean monthly anomalies in (a,d) rainfall in mm day^{-1} (b,d) frequency of rainy days in percentage, and (c,f)
 936 simple daily intensity index in mm day^{-1} . Superimposed on the shaded fields are (a,d) the AquaControl climato-
 937 logical rainfall (gray contours) and (b,c,e,f) the LandControl-AquaControl monthly rainfall anomalies (contours
 938 colored according to the colorbar in a). Top (a,b,c) is for the mean of the models with reduced heat capacity over
 939 land. Bottom (d,e,f) is for the average of the models with unchanged heat capacity.



940 FIG. 11. The annual cycle of LandControl minus AquaControl rainfall anomalies averaged zonally (Land-
 941 Control data over the continental sector only) and over (a) 10° - 15° N and (b) 10° - 15° S . The solid thin colored
 942 lines are individual models that followed protocol, the thick solid black line is their multi-model mean, and the
 943 light shading indicates a spread of ± 1 standard deviation. The dash-dotted lines are the two models that did not
 944 reduce heat capacity in the continental area.



945 FIG. 12. The effect of heat capacity on ascent profiles. (a) Vertical velocity omega profiles during SH summer
 946 in LandControl (DJF, shaded, averaged over the continental sector) and AquaControl (MAM contours, zonally
 947 averaged). Fields are the multi-model mean of the models that followed the full TRACMIP protocol in setting
 948 up land points. (b) Vertical velocity omega profiles during SH summer (as in a) but averaged over the latitude of
 949 tropical ascent and plotted for each individual model (solid for LandControl and dashed for AquaControl; note
 950 that we plot negative values both right and left of the vertical zero line, to allow for a cleaner comparison of the
 951 profile shape in LandControl (left) and AquaControl (right). (c) and (d): As in (a) and (b), but for the average
 952 of the two MetUM models, which did not reduce land's heat capacity. Southern Hemisphere summer season is
 953 therefore defined as MAM for both LandControl and AquaControl.